



Dynamics of foreign exchange implied volatility and implied correlation surfaces

S. Beer & H. Fink

To cite this article: S. Beer & H. Fink (2019): Dynamics of foreign exchange implied volatility and implied correlation surfaces, Quantitative Finance, DOI: [10.1080/14697688.2019.1575517](https://doi.org/10.1080/14697688.2019.1575517)

To link to this article: <https://doi.org/10.1080/14697688.2019.1575517>



Published online: 21 Feb 2019.



Submit your article to this journal 



Article views: 14



CrossMark

View Crossmark data 

Dynamics of foreign exchange implied volatility and implied correlation surfaces

S. BEER^{†*} and H. FINK^{‡§}

[†]Institute of Insurance Economics, University of St. Gallen, Tannenstrasse 19, CH-9000 St. Gallen, Switzerland

[‡]Department of Computer Science and Mathematics, Munich University of Applied Sciences, Lothstraße 64, D-80335 Munich, Germany

[§]Center for Quantitative Risk Analysis, Department of Statistics, Ludwig-Maximilians-University Munich, Akademiestraße 1/I, D-80799 Munich, Germany

(Received 7 March 2018; accepted 9 January 2019; published online 21 February 2019)

The prices of currency options expressed in terms of their implied volatilities and the implied correlations between foreign exchange rates at a given point in time depend on option delta and time to maturity. Implied volatilities and implied correlations likewise may thus be represented as a surface. It is well known that these surfaces exhibit both skew/smile features and term structure effects and their shapes fluctuate substantially over time. Using implied volatilities on three currency pairs as well as historical implied correlation values between them, we study the nature of these fluctuations by applying a Karhunen-Loève decomposition that is a generalization of a principal component analysis. We demonstrate that the largest share in the dynamics of these surfaces' fluctuations may be explained by exactly the same three factors, providing evidence of strong interdependences between implied correlation and implied volatility of global currency pairs.

Keywords: Foreign exchange rates; Implied volatility; Implied correlation; Dynamics; Interdependency; Karhunen-Loève decomposition

JEL Classification: C58, F31, G15

1. Introduction

The currency market is one of the world's largest and most liquid ones. According to latest statistics from the Bank for International Settlements' (BIS) triennial foreign exchange survey, the daily average in turnover of over-the-counter foreign exchange instruments[†] amounted to more than USD 5 trillion in 2016 (cf. www.bis.org). Transactions that are based on such instruments are carried out by nearly all branches of industry from Wall to main street, e.g. financial and governmental institutions, corporates, or private clients. Many market participants are therefore exposed to currency risk, and strategies to hedge or mitigate this risk are of interest to practitioners and researchers alike. If such strategies involve options of some kind, the following two aspects must be taken into consideration. Depending on the particular option type, one requires to have a detailed notion on

(i) the future evolution of volatility, and/or (ii) the prospective correlation between a strategy's single constituents, e.g. any two exchange rates. The latter is due to generally observable dependences between various global trading markets (cf. Roll 1988, Jorion 2000, Fink *et al.* 2017).

Contrary to the Black and Scholes framework, implied volatility that is usually derived from observed option prices is noticed to be non flat. It rather depends on both the strike level (or option delta) and time to maturity. The two-dimensional dependence is depicted by the implied volatility surface. Given the above context, considering this surface as a whole is especially important when pricing more complex options or when constructing hedging strategies for portfolios. Both usually rely on the usage of out-of-the-money or in-the-money options which cannot be adequately priced by employing historical spot or implied at-the-money volatility. In addition, multi-asset derivatives generally involving a basket of different individual securities require correlation between these constituents as one of the parameters for price setting. Here as well, values ignoring the aforementioned two-dimensional dependency are insufficient. Both volatility and correlation surfaces are consequently equally exceptionally important.

*Corresponding author. Email: simone.beer@unisg.ch

† Over-the-counter foreign exchange instruments are classified in five categories: spot transactions, outright forwards, foreign exchange swaps, currency swaps, and foreign exchange options.

Moreover, these surfaces' evolution over time captures the evolution of option prices. Market participants should therefore have a detailed knowledge on their dynamics. Over the past decades, a significant number of research papers have thus been concerned with investigating these fluctuations.

From the related literature stated in Section 2, however, we reveal three major research gaps which we will tackle within the scope of the present paper. Firstly, research on foreign exchange implied volatility surface dynamics remains rather limited until today. To the best of our knowledge, it is covered by Chalamandaris and Tsekrekos (2010) only. We aim to extend their work by considering both a longer and more recent time period that additionally includes different market regimes (i.e. crisis and non-crisis periods) and other currency pairs ignored so far. Secondly, no one has yet investigated the dynamics of implied correlation surfaces in the currency market using a higher dimensional principal component analysis. To name only a few, Butler and Cooper (1997) and more lately Wystup (2002) illustrate the computation of implied correlation using implied volatility on foreign exchange options, but they do not show any further application. In addition, they ignore the fact of correlation being dependent on both option delta and time to maturity, and thus refrain from constructing entire implied correlation surfaces (cf. Härdle and Silyakova 2012). Thirdly, we are unable to confirm the existence of any paper that analyses possible dependence structures between variations in implied volatility and implied correlation surfaces. To be more precise, we are interested in investigating whether the same underlying risk factors may drive both implied volatility and implied correlation.

In detail, we proceed as follows. Considering implied volatilities of the currency pairs EUR/JPY, EUR/USD and USD/JPY over a grid of fixed delta values and time to maturities, we first compute implied correlation between this set of currency pairs following Butler and Cooper (1997) and Wystup (2002). Based on Cont and da Fonseca (2002) and Härdle and Silyakova (2012), we then construct daily smooth implied volatility and implied correlation surfaces by employing a non-parametric smoothing procedure. Eventually, we study the dynamics of these surfaces according to Cont and da Fonseca (2002) and Chalamandaris and Tsekrekos (2010). Our goal is to provide a new contribution towards a more comprehensive understanding of the dynamics of foreign exchange implied volatilities and correlations.

The remainder of the paper is organized as follows. Section 2 is dedicated to reviewing prior literature related to our topic. The data set is introduced in Section 3, along with a descriptive analysis. In addition, the approach to compute implied correlation is presented. Afterwards, Section 4 covers the non-parametric smoothing methodology to construct daily smooth implied volatility and correlation surfaces. Finally, the Karhunen-Loëve decomposition that is used to analyse the surfaces' dynamics as well as its numerical implementation is briefly reviewed. Section 5 illustrates selected smooth surfaces. The empirical results are discussed in Sections 6 and 7, respectively. Section 8 concludes.

2. Related literature

Research on implied volatility which is extractable from observed option prices is first done by Latane and Rendleman (1976). They find it to be a better predictor of future realized volatility than estimators based on historical data. Subsequent research by Fleming *et al.* (1995) use an implied volatility index to forecast stock market volatility but also provide evidence of its enhanced forecasting performance compared to historical estimators. Analogous results are obtained by Christensen and Prabhala (1998) and Fleming (1998); and more lately by Dijk *et al.* (2014), Fernandes *et al.* (2014), Kim and Seo (2015) and Ma *et al.* (2016). The previous studies on equity volatility are expanded to include currency markets where similar conclusions are drawn (cf., e.g. Scott and Tucker 1989, Jorion 1995). In addition and more recently, Della and Tsiakas (2011) empirically analyse the predictive power of forward implied volatility for spot volatility. Using over-the-counter currency options, they find it to be a systematically biased predictor, overestimating movements in future spot implied volatility. Also related to this asset class, other studies apply market risk factors to forecast the cyclical behaviour of exchange rates (cf., e.g. Ahmed and Straetmans 2015), or investigate the predictive ability of foreign exchange rate volatility and its impact on the return of carry trade strategies (cf., e.g. Cenedese *et al.* 2014, Egbers and Swinkels 2015, Anatolyev *et al.* 2017).

By contrast, a different field of latest research does not evaluate the forecasting ability of implied volatility but investigates its dynamics. Whereas a considerable amount of literature is dedicated to the equity space, the work related to currency markets remains limited until today.

To start with, Fengler *et al.* (2002) apply a principal component analysis to identify two risk factors that explain the largest share in total variation with respect to the term structure of at-the-money DAX implied volatilities. A similar approach is taken by Alexander (2001), applied to at-the-money volatility smiles and skews of the FTSE 100 index. Alexander and Kaeck (2012) look at the dynamics of volatility time series of S&P 500 index returns and test non-affine as well as affine stochastic volatility option pricing models that incorporate jumps and a second stochastic variance factor. In addition, Li (2013) investigates the continuous-time dynamics of two volatility indices, VIX and VSTOXX, and further tests the inclusion of a nonlinear drift term when modelling the indices' price processes. Grossmann *et al.* (2014) employ a panel vector auto regressive model (PVAR) to study the dynamics of exchange rate volatility in the presence of economic shocks and report dynamic interrelationships between macroeconomic and financial variables, respectively, and exchange rate volatility. Magris *et al.* (2017) analyse implied volatility smile dynamics around jumps in the underlying price process based on intra-day S&P 500 index option data. Using the first three principal components to describe the implied volatility smile, they find a sudden change in the price of the underlying to lead to different implied volatility

smile dynamics in comparison to the absence of abrupt price changes.

A more comprehensive view on the dynamics of the whole implied volatility surface in an academic setting is first taken, amongst others, by Skiadopoulos *et al.* (1999). They investigate the number and shape of shocks that move S&P 500 implied volatility smiles and surfaces by applying a principal component analysis (PCA). Two components explaining about 60% of the variance are identified. These results are subsequently confirmed by Mixon (2002) who, however, indicates that three factors are sufficient to explain the majority of volatility movements for S&P 500 index options. Subsequently, using option data on the S&P 500 and the FTSE index, Cont and da Fonseca (2002) apply a PCA to these two indices' daily volatility surfaces and identify three factors that explain the surfaces' fluctuations over time. These results are confirmed by Fengler *et al.* (2003) who investigate the implied volatility surface dynamics along maturity slices for the DAX index using a common principal component analysis (CPC). Casse and Guidolin (2005) analyse the determinants of implied volatility surfaces computed from option prices on the Italian MIBO index by employing an exploratory analysis. Application to value at risk (VaR) and portfolio choice calculations illustrate the importance of their results. In a slightly different setting that focusses on the predictability of volatility surfaces, Chalamandaris and Tsekrekos (2010) document three factors that capture a large portion of daily variation in implied volatility surfaces in the currency market. These factors are subsequently applied to forecast the surfaces. Similarly, Bernales and Guidolin (2014) aim at predicting the implied volatility surface dynamics of equity options and find that time-variation in stock option volatility surfaces is best forecast by incorporating information from the surfaces' dynamics of the corresponding index. Dempsey and Tanha (2016) report on the dynamics of the Australian SPI 200 implied volatility surfaces using a PCA and mostly confirm prior results. In summary, research on the dynamics of implied volatility surfaces consistently confirm that the three risk factors *level*, *term structure* and *convexity* together account for the largest share in variability over time.

The concept of implied volatility and its widespread use motivates researchers to also consider correlation derived from (basket) options. This leads to the notion of implied correlation. The main assumption underlying this approach is that option prices could also be employed to measure the future degree of correlation between two assets' returns, similar to implied volatility capturing prospective realized return volatility.

Within the scientific community, particular attention is given to implied correlation in the equity space. However, for equities, computing both implied correlation indices and surfaces requires reliable bivariate option prices on all index components. To overcome this obstacle, equal implied correlation for all index constituents (*equicorrelation*) is usually assumed. Employing the aforementioned assumption, the CBOE is the first exchange to start computing implied correlation indices for the S&P 500 from 2009. These indices aim at measuring the average expected dependence of the market (CBOE 2017). Referring to an academic setting, Skintzi and

Refenes (2005) and Linders and Schoutens (2014) propose to construct an implied equity correlation index and analyse its dynamics over time. A similar approach is taken by Fink and Geppert (2017) who build an implied correlation index for the German DAX index, investigate the international dependencies between equity, volatility and correlation indices and provide evidence of implied correlation being able to improve implied volatility forecasting. Härdle and Silyakova (2012) consider implied correlation to depend on both time to maturity and strike levels - just as for implied volatility - and compute daily implied correlation surfaces based on the equicorrelation assumption. Applying a dynamic semi-parametric factor model, they find three factors that influence the surfaces' shapes the most over time.

The literature cited beforehand provides important insights into implied equity correlation. The specific literature on implied correlation in currency markets is considerably more restricted. It mainly focuses on analysing the forecasting performance of implied correlation compared to measures based on historical time series data. Bodurtha and Shen (1995) are one of the first to study correlation implied in currency and cross-currency options. Using daily data on dollar-mark, dollar-yen and mark-yen exchange-traded options, implied correlation is computed. They subsequently evaluate both the information content and the predictive power of their correlation estimates and find that implied correlation well explains future realized correlation. Similar results are provided by Siegel (1997), Campa and Chang (1998) and Lopez and Walter (2000). They also study the forecasting performance of implied correlation computed from option data on exchange rates. The performance is analysed by comparing the option-based measure of correlation to alternative correlation estimates based on historical, time series observations. Compared to traditional historical-based estimates, they find implied correlation to be significantly superior in terms of predicting future realized correlation since it contains information that is not included in past data. More recently, however, Mueller *et al.* (2017) focus on a different research topic, that is to say, correlation risk premium. They find evidence of priced correlation risk in foreign exchange risk premia and analyse potential underlying economic factors driving this risk premium.

Another field of research provides evidence on increased stock return correlation during periods of generally observable low returns. For example, Roll (1988) analyse the international crash of October 1987 and Jorion (2000) investigates the failure of Long-Term Capital Management (LTCM) in 1998. Both find a sharp increase in overall asset return correlation in crisis periods, both within and across (intercontinental) financial markets. More recently, Jung and Maderitsch (2014) detect strong evidence of volatility transmission between international financial markets during market turmoil. Similar results are obtained by Clemens *et al.* (2015) who report significant volatility spillovers in global foreign exchange, equity and bond markets, and Fink *et al.* (2017) who confirm the existence of global dependence regimes between North-American, European and Asian equity as well as implied volatility indices.

3. Data set

3.1. The foreign exchange market

We denote the foreign exchange conversion rate between currencies m and n at time t by $S_{m/n,t}$ ($m \neq n$). It indicates the specific amount of currency n that is required to purchase one unit of currency m at time t . Supposing you buy a currency pair, currency m is then called the base currency and currency n is termed the quoted currency.

In choosing an appropriate set of currencies, we consider liquidity as the main criterion of selection (cf. www.bis.org for an overview of the daily average turnover of over-the-counter foreign exchange instruments by currency in 2016). In addition, we limit ourselves to three valuta, allowing the applicability of the currency triangular approach. Provided its validity, it ensures the absence of any triangular arbitrage opportunities which is a necessary prerequisite for the computation of implied correlation (cf. Section 3.3). We eventually assume $m, n \in \{\text{EUR}, \text{USD}, \text{JPY}\}$. Please note that each of these three major currencies may act as both the base and the quoted currency. We are thus faced with six possible currency pair combinations. However, we opt for the three exchange rates EUR/JPY , EUR/USD and USD/JPY due to the following two reasons: (i) we require implied volatility quotes in the empirical part, and the standard quoting convention in the interbank foreign exchange market (FOREX) is precisely based on these three rates, (ii) we are able to build an admissible currency triangle by applying these three exchange rates.

The period under investigation ranges from January 4th, 2006 to September 1st, 2017, covering 3,041 trading days (due to some glitch in the data set, August 17th, 2007 had to be excluded). The start of the sample coincides with the first-time availability of daily quotes for both the full range of different delta values and time to maturities as defined in Section 3.2. The data set also includes the most recent financial crisis that reached its peak in 2008. Its influence on the empirical results is clearly observable (cf. Sections 6 and 7). The present section looks back at the foreign exchange market of that particular year by outlining the economic and political events that were most striking. In doing so, we focus on three important occasions.

On September 16th, the bankruptcy of Lehman Brothers which was the fourth-largest investment bank in the United States launched a period of further bank failures, both in the United States and Europe. This was followed by a worldwide massive reduction in the value of financial assets and eventually resulted in a global financial and economic crisis. On October 24th, many of the world's most important stock exchanges suffered the worst drop in their recent history, declining by around 10%. The U.S. and Japanese leading indices did not experience such a dramatic decline; the Dow Jones Industrial Average, for example, only fell by roughly 3%. This led to a situation in which the U.S. dollar (USD) and the Japanese yen (JPY) increased their value against other major currencies such as the euro (EUR) since investors were seeking (relatively) safe haven investments. Both the upper and the lower image of figure 1 displays the abruptly massive devaluation of the EUR against both the JPY and the USD



Figure 1. EUR/JPY , USD/JPY and EUR/USD historical exchange rates from January 4th, 2006 to September 1st, 2017.

on October 27th. The EUR/USD currency pair fell from 1.60 in September to 1.24 by the end of November. However, the EUR recovered again as the recession in the U.S. economy gathered pace in the first quarter of 2009. The USD soon lost its strength, not only against the EUR but also against the JPY . The latter currency strengthened against the USD to a level not seen for 13 years. In addition, two other important occasions heavily hit financial markets. On January 15th, the Swiss National Bank (SNB) discontinued the minimum exchange rate of $\text{CHF} 1.20$ per EUR and simultaneously decreased the

Table 1. Example of foreign exchange implied volatility quotation for the *EUR/USD* currency pair on December 1st, 2014.

Expiry	ATM	10 Delta Risk Reversal	10 Delta Butterfly
1W	10.460	1.210	0.447
1M	8.407	1.577	0.424
3M	8.385	2.070	0.627
6M	8.258	2.210	0.794
1Y	8.315	2.288	0.981
2Y	8.395	1.888	0.931

interest rate on sight deposit account balances to a new level of -0.75% . As the SNB's approach was mainly interpreted as a sign of the European Central Bank (ECB) soon announcing a quantitative easing programme, this led to immediate and strong reactions in currency markets (with observed spillovers to equity markets). To be more precise, the *EUR* considerably depreciated against both the *JPY* and the *USD* (cf. upper and lower image of figure 1).

3.2. Volatility quotation

In the foreign exchange market, implied volatilities, apart from the at-the-money volatility $\sigma_{t,j}(ATM, \tau_j)$, are usually not quoted directly but rather via: (i) the risk reversals $\sigma_{t,j}^{RR}(x_i\Delta, \tau_j)$ using $x_i\Delta$ call and put options, and (ii) the butterflies $\sigma_{t,j}^{BF}(x_i\Delta, \tau_j)$ with $x_i\Delta$ wings. Via Bloomberg, we collect historical at-the-money, risk reversal and butterfly quotes for three currency pairs - *EUR/JPY*, *EUR/USD* and *USD/JPY* - over a grid of delta values $x\Delta$ and time to maturities τ . Maturities are between one week and two years, while for each term and derivative type *ATM*-, 10Δ - and 25Δ -quotes are available (cf. table 1 for an example of this quotation). All quotes are mid levels of bid/ask quotes at the close of trading and refer to European-style options traded over-the-counter. In particular, we have

$$\begin{aligned} x &\in \{10, 25, ATM\} \Delta \quad \text{and} \\ \tau &\in \left\{ \frac{1}{48}, \frac{1}{24}, \frac{1}{16}, \frac{1}{12}, \frac{1}{6}, \frac{1}{4}, \frac{1}{3}, \frac{1}{2}, \frac{3}{4}, 1, 2 \right\} \text{ years}, \end{aligned}$$

such that the particular notation for a single implied volatility quote at time t is $\sigma_{t,j}(x_i\Delta, \tau_j)$ (ignoring the type of quote for the moment), where $j = 1, \dots, J$ and $i = 1, \dots, I$ (both independent of day t).

Using the obtained market quotes and given a term structure of interest, single implied volatilities for 10Δ and 25Δ calls and puts and eventually a discrete volatility surface can be computed. In doing so, we apply the standard market procedure outlined in Bloomberg (2009). For more literature on this topic, we refer to Bisesti *et al.* (2005), Reiswich and Wystrup (2012) and therein.

The at-the-money strike is usually defined as the strike for which a straddle that involves the simultaneous purchase of both a put and a call on the same underlying, with identical strikes and expiration dates will have a delta of zero, i.e. is delta neutral (Bloomberg 2009). For simplicity, we shall assume that the at-the-money volatilities correspond to a delta of 50. Even though this is usually not correct, it would influence our analysis to come only on an axis-scaling level.

On the Bloomberg system, for a fixed time to maturity τ_j , the risk reversal quote is defined as the volatility of a call option minus the volatility of a put option on the particular exchange rate's base currency, where both options have equal absolute deltas. For example, the risk reversal quotation $\sigma_{t,j}^{RR}(10\Delta, \tau_j)$ returns the difference between the implied volatility $\sigma_{t,j}^C(10\Delta, \tau_j)$ of a call with a delta of 10 and the implied volatility $\sigma_{t,j}^P(10\Delta, \tau_j)$ of a put with a delta of -10 , i.e.

$$\sigma_{t,j}^{RR}(10\Delta, \tau_j) = \sigma_{t,j}^C(10\Delta, \tau_j) - \sigma_{t,j}^P(10\Delta, \tau_j). \quad (1)$$

The 10Δ butterfly $\sigma_{t,j}^{BF}(10\Delta, \tau_j)$, expressed in volatility terms, reads as follows:

$$\sigma_{t,j}^{BF}(10\Delta, \tau_j) = \frac{\sigma_{t,j}^C(10\Delta, \tau_j) + \sigma_{t,j}^P(10\Delta, \tau_j)}{2} - \sigma_{t,j}(ATM, \tau_j). \quad (2)$$

Therefore, for a given time to maturity τ_j , the two implied volatilities $\sigma_{t,j}^C(10\Delta, \tau_j)$ and $\sigma_{t,j}^P(10\Delta, \tau_j)$ can then be computed by simply solving the following linear system:

$$\begin{aligned} \sigma_{t,j}^C(10\Delta, \tau_j) &= \sigma_{t,j}(ATM, \tau_j) + \frac{1}{2}\sigma_{t,j}^{RR}(10\Delta, \tau_j) \\ &\quad + \sigma_{t,j}^{BF}(10\Delta, \tau_j); \\ \sigma_{t,j}^P(10\Delta, \tau_j) &= \sigma_{t,j}(ATM, \tau_j) - \frac{1}{2}\sigma_{t,j}^{RR}(10\Delta, \tau_j) \\ &\quad + \sigma_{t,j}^{BF}(10\Delta, \tau_j). \end{aligned} \quad (3)$$

The two formulas depicted in (3) allow calculating the 10Δ volatilities $\sigma_{t,j}^C(10\Delta, \tau_j)$ and $\sigma_{t,j}^P(10\Delta, \tau_j)$, respectively, for market quotes as given in table 1. Implied volatilities for a delta of 25 shall be computed accordingly. Taking various time to maturities τ_j into account, a discrete implied volatility surface can eventually be constructed.

3.3. Implied correlation computation

We again focus on the set of three currency pairs as stated in Section 3.1 and use the following notation at time t . The *EUR/JPY* and *EUR/USD* exchange rates are denoted by $S_{\text{€/¥},t}$ and $S_{\text{€/$},t}$, respectively, while $S_{\$/\text{¥},t}$ refers to the *USD/JPY* exchange rate. Here too, for simplicity (cf. Section 3.2), the type of quote is initially ignored. It then holds that $\sigma_{\text{€/¥},t,j}(x_i\Delta, \tau_j)$, $\sigma_{\text{€/$},t,j}(x_i\Delta, \tau_j)$ and $\sigma_{\$/\text{¥},t,j}(x_i\Delta, \tau_j)$ state the implied volatility quotes for the *EUR/JPY*, the *EUR/USD* and the *USD/JPY* exchange rate for a given $x_i\Delta$ and τ_j , respectively. Furthermore, the three triangular parity conditions ensuring the existence of no-arbitrage read as follows:

$$S_{\$/\text{¥},t} = \frac{S_{\text{€/¥},t}}{S_{\text{€/$},t}}, \quad (4)$$

$$S_{\text{€/$},t} = \frac{S_{\text{€/¥},t}}{S_{\$/\text{¥},t}}, \quad (5)$$

and

$$S_{\text{€/¥},t} = S_{\text{€/$},t} \cdot S_{\$/\text{¥},t}, \quad (6)$$

respectively (cf., e.g. Gradojevic and Gencay 2014). Provided that implied volatility quotes on all three aforementioned

pairs are available and assuming that the no-arbitrage condition holds, implied correlation between any two of these three pairs may be calculated. In doing so, we closely follow Butler and Cooper (1997) and Wystup (2002). Here, the above-stated three triangular parity conditions form the basis for computation.

We firstly address the situation in which a particular currency rate is obtained by dividing two spot exchange rates, as shown in equations (4) and (5). Please note that we illustrate the detailed derivation of implied correlation for the first case only, i.e. the *USD/JPY* exchange rate. The formula resulting from the latter is subsequently specified. Due to its close similarity with the first, we refrain from demonstrating the approach. To begin with, we define the rate of change in the *USD/JPY* exchange rate at time t by

$$r_{\$/\text{¥},t} = \ln \left(\frac{S_{\$/\text{¥},t}}{S_{\$/\text{¥},t-1}} \right). \quad (7)$$

If we recall equation (4), it clearly follows that equation (7) may alternatively be presented as

$$r_{\$/\text{¥},t} = \ln \left(\frac{\frac{S_{\$/\text{¥},t}}{S_{\$/\text{¥},t-1}}}{\frac{S_{\$/\text{¥},t-1}}{S_{\$/\text{¥},t-1}}} \right). \quad (8)$$

If the expression in parentheses is now arranged, we obtain

$$\begin{aligned} r_{\$/\text{¥},t} &= \ln \left(\frac{\frac{S_{\$/\text{¥},t}}{S_{\$/\text{¥},t-1}}}{\frac{S_{\$/\text{¥},t-1}}{S_{\$/\text{¥},t-1}}} \right) = \ln \left(\frac{S_{\$/\text{¥},t}}{S_{\$/\text{¥},t-1}} \right) - \ln \left(\frac{S_{\$/\text{¥},t-1}}{S_{\$/\text{¥},t-1}} \right) \\ &= r_{\$/\text{¥},t} - r_{\$/\text{¥},t-1}. \end{aligned} \quad (9)$$

It then holds that

$$\text{Var}(r_{\$/\text{¥},t}) = \text{Var}(r_{\$/\text{¥},t}) + \text{Var}(r_{\$/\text{¥},t-1}) - 2 \cdot \text{Cov}(r_{\$/\text{¥},t}, r_{\$/\text{¥},t-1}). \quad (10)$$

Given a particular exchange rate, let us subsequently replace the variance of its rate of change with the expected squared deviation, that is to say, with its implied volatility quote. We thus obtain

$$\begin{aligned} \sigma_{\$/\text{¥},t}^2 &= \sigma_{\$/\text{¥},t}^2 + \sigma_{\$/\text{¥},t-1}^2 - 2 \cdot \text{Cov}(r_{\$/\text{¥},t}, r_{\$/\text{¥},t-1}) \\ &= \sigma_{\$/\text{¥},t}^2 + \sigma_{\$/\text{¥},t-1}^2 - 2 \cdot \sigma_{\$/\text{¥},t} \cdot \sigma_{\$/\text{¥},t-1} \cdot \rho_{\$/\text{¥},t-\$/\text{¥},t-1}. \end{aligned} \quad (11)$$

Rearranging equation (11) and additionally taking into account the dependence of implied volatility on both a given delta $x_i\Delta$ and time to maturity τ_j yields the implied correlation between *JPY* and *USD* at time t having *EUR* as numerator. It is defined as

$$\begin{aligned} \rho_{\$/\text{¥}-\$/\text{¥},t,ij}(x_i\Delta, \tau_j) &= \frac{\sigma_{\$/\text{¥},t,ij}^2(x_i\Delta, \tau_j) + \sigma_{\$/\text{¥},t,ij}^2(x_i\Delta, \tau_j) - \sigma_{\$/\text{¥},t,ij}^2(x_i\Delta, \tau_j)}{2\sigma_{\$/\text{¥},t,ij}(x_i\Delta, \tau_j)\sigma_{\$/\text{¥},t,ij}(x_i\Delta, \tau_j)}. \end{aligned} \quad (12)$$

Accordingly, implied correlation between *EUR* and *USD* at time t using *JPY* as denominating currency is given by

$$\begin{aligned} \rho_{\$/\text{¥}-\$,\$/\text{¥},t,ij}(x_i\Delta, \tau_j) &= \frac{\sigma_{\$/\text{¥},t,ij}^2(x_i\Delta, \tau_j) + \sigma_{\$/\text{¥},t,ij}^2(x_i\Delta, \tau_j) - \sigma_{\$/\text{¥},t,ij}^2(x_i\Delta, \tau_j)}{2\sigma_{\$/\text{¥},t,ij}(x_i\Delta, \tau_j)\sigma_{\$/\text{¥},t,ij}(x_i\Delta, \tau_j)}. \end{aligned} \quad (13)$$

Next, we focus on the *EUR/JPY* exchange rate, being the product of two spot exchange rates. It is expressed in equation (6). Here, the rate of change at time t is given by

$$\begin{aligned} r_{\$/\text{¥},t} &= \ln \left(\frac{S_{\$/\text{¥},t}}{S_{\$/\text{¥},t-1}} \cdot \frac{S_{\$/\text{¥},t}}{S_{\$/\text{¥},t-1}} \right) = \ln \left(\frac{S_{\$/\text{¥},t}}{S_{\$/\text{¥},t-1}} \right) \\ &\quad + \ln \left(\frac{S_{\$/\text{¥},t}}{S_{\$/\text{¥},t-1}} \right) = r_{\$/\text{¥},t} + r_{\$/\text{¥},t-1}. \end{aligned} \quad (14)$$

It now follows that

$$\sigma_{\$/\text{¥},t}^2 = \sigma_{\$/\text{¥},t}^2 + \sigma_{\$/\text{¥},t-1}^2 + 2 \cdot \sigma_{\$/\text{¥},t} \cdot \sigma_{\$/\text{¥},t-1} \cdot \rho_{\$/\text{¥}-\$/\text{¥},t}. \quad (15)$$

If we finally rearrange equation (11) and again consider the dependence of implied volatility on both a given delta $x_i\Delta$ and time to maturity τ_j , implied correlation between the *EUR/USD* and *USD/JPY* exchange rate at time t reads as follows:

$$\begin{aligned} \rho_{\$/\text{¥}-\$,\$/\text{¥},t,ij}(x_i\Delta, \tau_j) &= \frac{-\sigma_{\$/\text{¥},t,ij}^2(x_i\Delta, \tau_j) - \sigma_{\$/\text{¥},t,ij}^2(x_i\Delta, \tau_j) + \sigma_{\$/\text{¥},t,ij}^2(x_i\Delta, \tau_j)}{2\sigma_{\$/\text{¥},t,ij}(x_i\Delta, \tau_j)\sigma_{\$/\text{¥},t,ij}(x_i\Delta, \tau_j)}. \end{aligned} \quad (16)$$

To conclude, for each day t , we additionally take into consideration the type of option. The implied volatility quotes $\sigma_{t,ij}^C(x_i\Delta, \tau_j)$ and $\sigma_{t,ij}^P(x_i\Delta, \tau_j)$ for a range of Δ values and time to maturities τ , where $j = 1, \dots, J$ and $i = 1, \dots, I$ (cf. Section 3.2), may thus be used to compute implied correlation according to equations (12), (13) and (16), respectively. We repeat this approach for any of the three correlation pairs defined above, referring to the same grid of delta values Δ and time to maturities τ as for implied volatilities.

4. Methodology

4.1. Surface construction

We follow Cont and da Fonseca (2002) and build a daily time series of smooth implied volatility surfaces denoted by $\{IV_t(\Delta, \tau)\}_{t=1, \dots, T=3,041}$ for each of the three currency pairs. In doing so, we employ a non-parametric Nadaraya-Watson estimator with a Gaussian kernel, i.e.

$$IV_t(\Delta, \tau) = \frac{\sum_{i=1}^I \sum_{j=1}^J \sigma_{t,ij}(\Delta_i, \tau_j) g(\Delta - \Delta_i, \tau - \tau_j)}{\sum_{i=1}^I \sum_{j=1}^J g(\Delta - \Delta_i, \tau - \tau_j)}, \quad \Delta \in [0.1, 0.9], \quad \tau \in \left[\frac{1}{48}, 2 \right] \quad (17)$$

$$g(x, y) = (2\pi)^{-1} \exp \left\{ -\frac{x^2}{2h_1} - \frac{y^2}{2h_2} \right\}, \quad x, y \in \mathbb{R}, \quad (18)$$

with bandwidth parameters h_1 and h_2 . It holds that $t = 1, \dots, T = 3,041, i = 1, \dots, I$ and $j = 1, \dots, J$; the latter two refer to the indices of observations of implied volatility quotes at day t but are independent of it. To ensure the proper application of the estimator, we invoke the put-call-parity and transform the put deltas into corresponding call deltas, i.e. a put delta corresponds to a call delta minus 1. This approach results in a monotonically increasing interval of delta values for a given time to maturity.

In literature, there exists a variety of methods that can be applied to determine the optimal bandwidth parameters h_1 and h_2 , e.g. the application of a cross-validation criterion or the employment of an adaptive bandwidth estimator (cf. Härdle 1990, Gasser *et al.* 1991, Brockmann *et al.* 1993). However, we would like to exclude the potential influence of a daily change in the smoothing parameters and therefore take a different approach. Moreover, any reasonable smoothing parameters lead to basically the same results. In detail, we proceed as follows. To begin with, we decide to restrict ourselves to one single currency rate and opt for the EUR/JPY exchange rate. Furthermore, our approach is exclusively applied to the first available implied volatility quotes in the data set, i.e. January 4th, 2006. Next, we generate a sequence of smoothing parameters, where $h_1 = h_2 \in [0.001, 0.090]$ in steps of 0.005. Please note that we consider any combination of the two smoothing parameters. Precisely speaking, step by step, we fix h_1 and let h_2 vary from 0.001 to 0.090. The subsequent application of the non-parametric Nadaraya-Watson estimator using a Gaussian kernel to the two parameters' sequences results in a range of smooth EUR/JPY implied volatility surfaces. To finally determine the optimal bandwidth parameters, we classify the resulting surfaces in 18 groups according to the fixed h_1 value. Within each group, we then compute the root mean square error (RMSE)[†] between the original implied volatility quotes available for a range of Δ values and time to maturities τ and the corresponding smoothed quotes, and subsequently take the mean of the RMSE values for each group. We find $h_1 = 0.031$ to match the average RMSE across all 18 groups, and, having chosen $h_1, h_2 = 0.031$ to report the mean RMSE within the set of fixed h_1 values. To sum up, we opt for $h_1 = h_2 = 0.031$ to be the optimal choice for the two bandwidth parameters.

We now turn our attention to implied correlation, and again build daily time series of smooth surfaces that are denoted by $\{IC_t(\Delta, \tau)\}_{t=1, \dots, T=3,041}$. In doing so, we apply the same non-parametric Nadaraya-Watson estimator as defined in equations (17) and (18), respectively, to EUR/JPY-EUR/USD, EUR/JPY-USD/JPY and EUR/USD-USD/JPY correlation quotes as computed in Section 3.3. In line with implied volatilities, we use the identical grid of

[†]The measure is defined as follows:

$$\text{RMSE} = \sqrt{\frac{1}{N} \sum_{i=1}^I \sum_{j=1}^J (\sigma_{i,j}(\Delta_i, \tau_j) - \hat{\sigma}_{i,j}(\Delta_i, \tau_j))^2};$$

where N is the number of available implied volatility quotes σ for a range of Δ values and time to maturities τ at day t . Please note that t is fixed at January 4th, 2006. Smoothed implied volatilities using particular bandwidth parameters h_1 and h_2 are denoted by $\hat{\sigma}$.

delta values Δ and time to maturities τ . Focusing on the EUR/JPY-EUR/USD implied correlation quotes on January 4th, 2006, we follow the previously described approach and again find $h_1 = h_2 = 0.031$ to be the optimal choice for the two bandwidth parameters.

4.2. The Karhunen-Loève decomposition

The Karhunen-Loève decomposition is a generalization of the principal component analysis (PCA) with respect to higher dimensional random fields. Let $\{IV_t(\Delta, \tau)\}_{t \in \mathbb{R}}$ and $\{IC_t(\Delta, \tau)\}_{t \in \mathbb{R}}$ denote stochastic processes that represent the evolution of an implied volatility and an implied correlation surface over time. Following the approach of Cont and da Fonseca (2002) and Härdle and Silyakova (2012), we aim to decompose the volatility process via

$$IV_t(\Delta, \tau) \approx IV_0(\Delta, \tau) \exp \left[\sum_{k=1}^K x_k^{IV}(t) f_k^{IV}(\Delta, \tau) \right], \quad (19)$$

while for the correlation dynamics we adjust their methodology by using daily arctanh variations instead of logarithmic variations to obtain

$$IC_t(\Delta, \tau) \approx IC_0(\Delta, \tau) \tanh \left[\sum_{k=1}^K x_k^{IC}(t) f_k^{IC}(\Delta, \tau) \right]. \quad (20)$$

The non-stochastic surface-valued functions f_k^{IV} and f_k^{IC} , respectively, are called eigenmodes or eigensurfaces; while the real-valued stochastic processes x_k^{IV}, x_k^{IC} are projections of the initial surfaces' log/arctanh-variations on the former. Numerically, the above two approximations can be obtained by expanding each eigenmode by a sum of L smooth surface-valued basis functions h_l , where $l = 1, \dots, L$. We decide to choose $L = 182$ cubic two-dimensional B-splines with equidistantly distributed knots.

Afterwards, a generalized eigenvalue problem (derived from the original surfaces' daily variations and the above-stated basis functions) has to be solved numerically to get the approximations in equations (19) and (20), respectively (cf. Cont and da Fonseca 2002 for a detailed explanation). The eigenmodes can then be ordered by their %-wise share of the original surfaces' daily variations.

5. Surface shapes

5.1. Volatilities

Figure 2 shows some examples of how daily smooth implied volatility surfaces may fluctuate over time. In any case, it seems obvious that the smile in foreign exchange markets exhibits a greater variety of different shapes than the smile in the equity space. The latter is generally characterized by a decreasing implied volatility as the strike price rises. Referring to currency options, the smile may change skewness as time goes by, become almost flat, considerably increase at its wings or even invert its convexity and transform itself into a

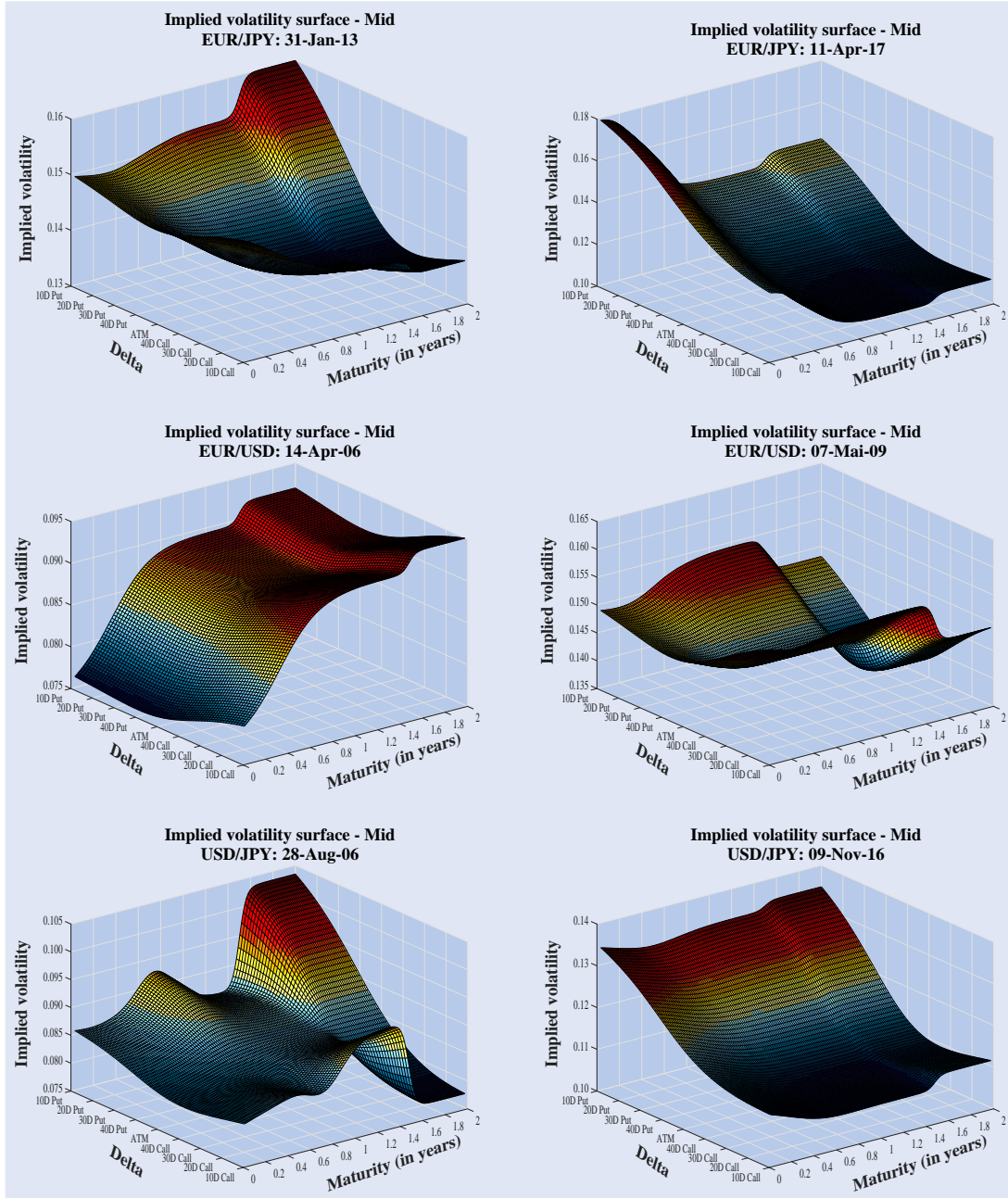


Figure 2. Selected implied volatility surfaces for the three currency pairs *EUR/JPY*, *EUR/USD* and *USD/JPY* (using implied volatility mid market quotes).

smirk (cf. Rebonato 2004 for a very good overview). The presented surfaces support these arguments for the most part. To understand the magnitude of the smile's shape, the following fact is worth noting: as outlined in Section 3.2, the curvature and the slope of the smile can be derived from a sequence of risk reversal and butterfly quotes for a given delta. For each delta, both quotes reveal the difference in implied volatilities for the two options that build the respective strategy. For example, a positive risk reversal quote of 3% indicates that an out-of-the-money put is - expressed in terms of implied volatility - cheaper than an out-of-the-money call. Hence, the implied volatility of the put is 3% below the implied volatility of the call with respect to the particular delta the quote refers to. If the butterfly quote is positive, an at-the-money option is

comparatively cheaper than an out-of-the-money option (cf. Cooper and Talbot 1999, Rebonato 2004). In fact, Cooper and Talbot (1999) analyse 25 Δ risk reversal and 25 Δ butterfly quotes on a daily basis for the *USD/JPY* exchange rate in 1998. They discover the first to considerably vary both in level and sign, while the latter is found to move around mostly positive values.

Based on the time series of daily smooth implied volatility surfaces denoted by $\{IV_t(\Delta, \tau)\}_{t=1, \dots, T = 3,041}$, we then compute the sample average of these surfaces for each currency pair over the entire period under investigation. The results are depicted on the left-hand side of figure 3, where the average implied volatility is presented as a function of option delta (Δ) and time to maturity (τ) in years. We observe an

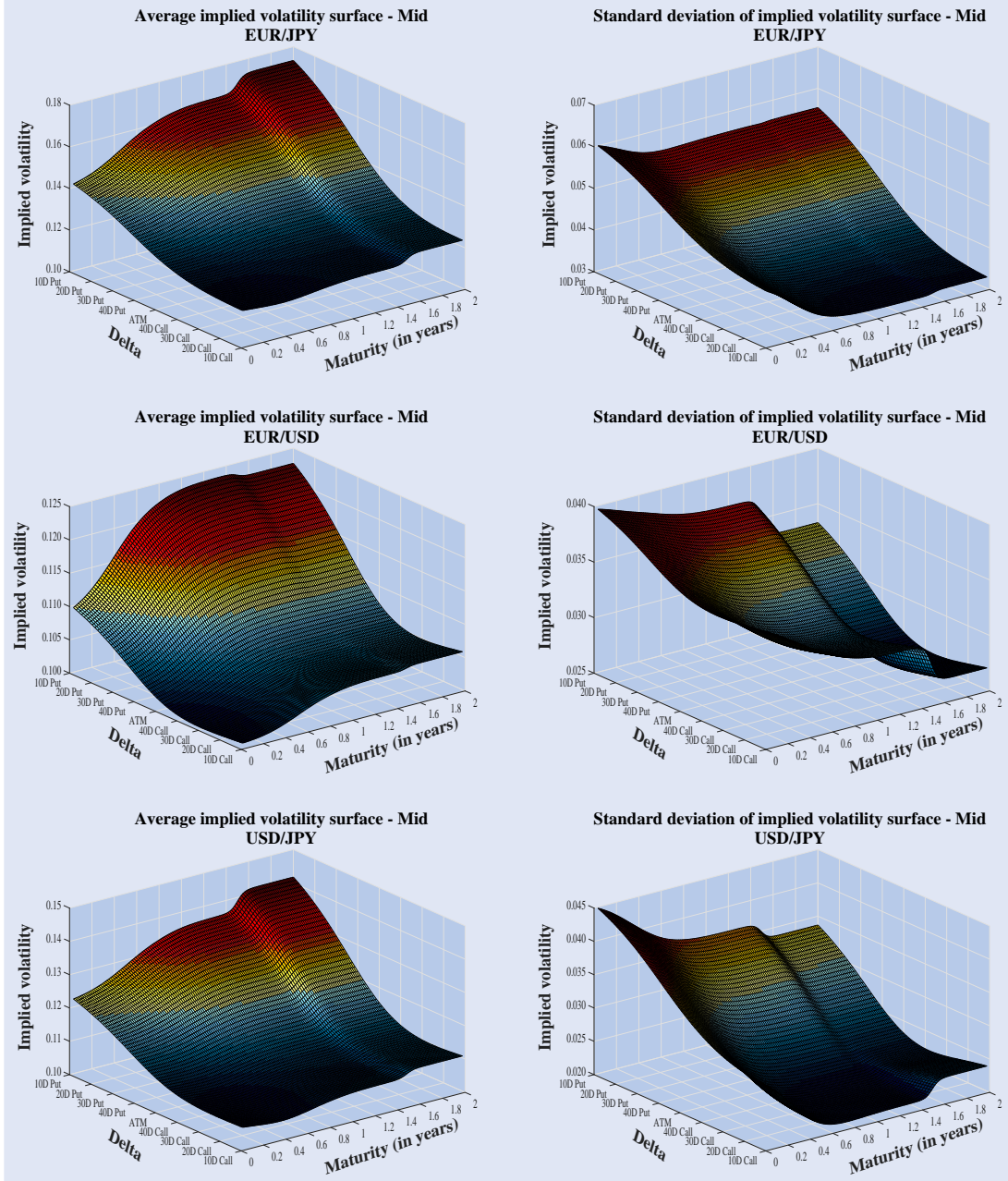


Figure 3. Left: average profile of EUR/JPY, EUR/USD and USD/JPY implied volatility surface (using implied volatility mid market quotes). Right: daily standard deviation of EUR/JPY, EUR/USD and USD/JPY implied volatilities (based on mid market quotes) as a function of option delta and time to maturity.

upward sloping term structure and a pronounced skew for all of the three surfaces. The sample standard deviation of implied volatilities, as illustrated on the right-hand side of figure 3, implies that each of the three surfaces is not static but shows distinct fluctuations around its average profile over time. There is strong evidence of variability in implied volatilities across different option deltas, i.e. we find smiles to change heavily in shape as time goes by. Precisely speaking, we observe the daily standard deviation of implied volatility to be as large as a third or quarter, respectively, of its representative value regarding out-of-the-money options. This has important implications for option pricing. Cont and da Fonseca (2002) report similar findings.

5.2. Correlations

Figure 4 provides a first impression of how implied correlation surfaces might behave over time. It is immediately noticeable that the different shapes are very similar to what has already been found for implied volatility surfaces in general and in particular for currency markets. Since the approach to derive implied correlation values (cf. Section 3.3) is highly non-linear, the correlation surfaces' behaviour is, however, not clear ex-ante. To be more precise, the surfaces exhibit smiles that change their particular skewness over time. If one additionally analyses the surfaces' term structure, no clear pattern is observable. It may be downward or upward sloping,

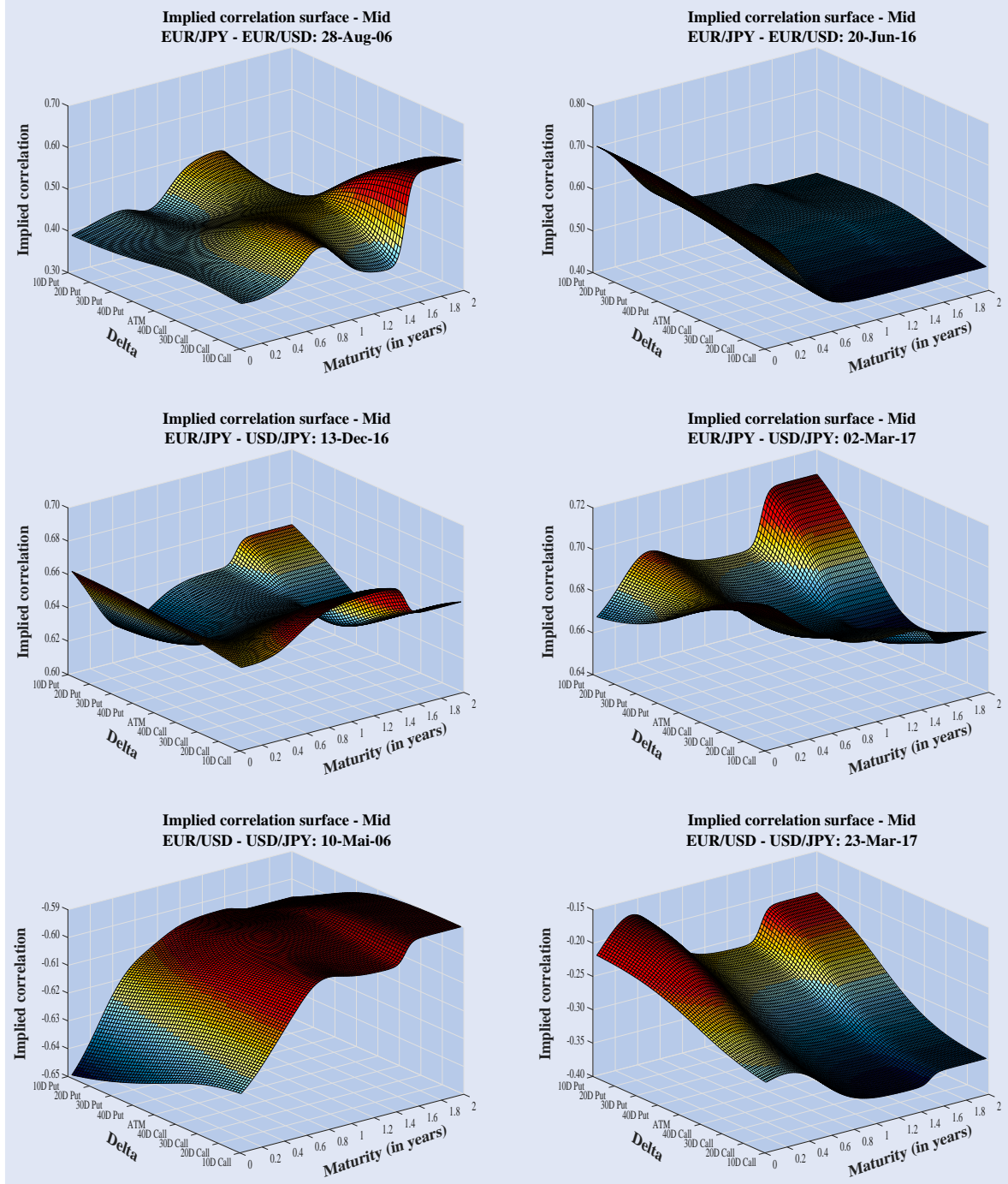


Figure 4. Selected implied correlation surfaces for the three correlation pairs *EUR/JPY-EUR/USD*, *EUR/JPY-USD/JPY* and *EUR/USD-USD/JPY* (based on implied volatility mid market quotes).

almost flat or move across time to maturity without displaying an identifiable trend. Again, this is in line with the above described findings for the implied volatility surface.

Based on the time series of daily smooth implied correlation surfaces denoted by $\{IC_t(\Delta, \tau)\}_{t=1, \dots, T = 3,041}$, we compute the sample average of these surfaces for each correlation pair using the entire period under investigation. The images on the left-hand side of figure 5 illustrate the results. Please note that the average implied correlation is presented as a function of option delta (Δ) and time to maturity (τ) in years. Here as well, we find an upward sloping term structure for

the average profile of the *EUR/JPY-EUR/USD* implied correlation surface, while we observe it to be almost flat for the average *EUR/USD-USD/JPY* correlation surface. By contrast, the term structure for the correlation pair *EUR/JPY-USD/JPY* is slightly U-shaped. In line with the previously reported results for the average implied volatility surface, we observe a pronounced skew for the mean *EUR/JPY-USD/JPY* and *EUR/USD-USD/JPY* implied correlation. The average profile of the *EUR/JPY-EUR/USD* implied correlation surface, however, displays an inverted smile with decreasing correlation values at the smile's wings. The sample standard

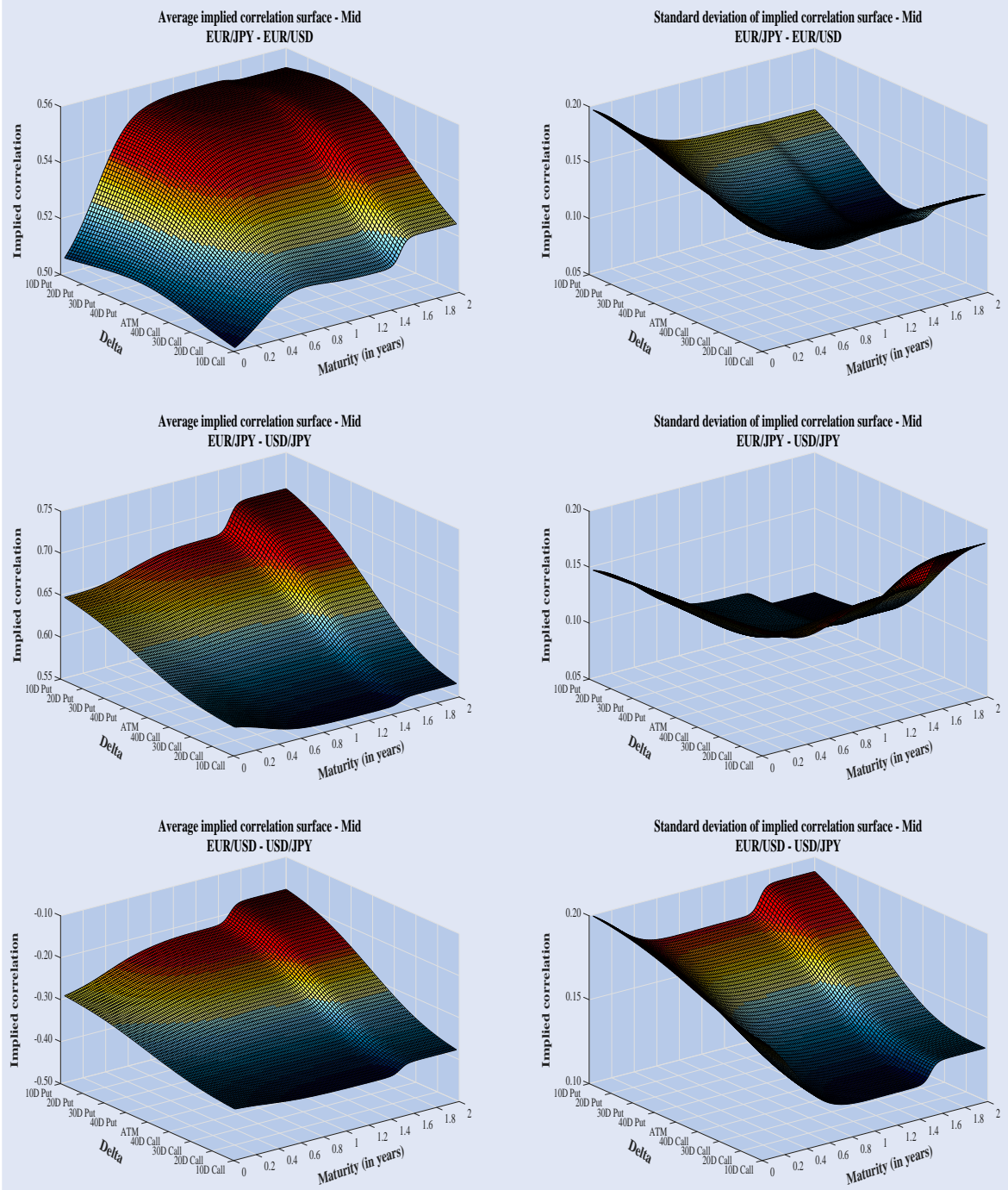


Figure 5. Left: average profile of EUR/JPY-EUR/USD, EUR/JPY-USD/JPY and EUR/USD-USD/JPY implied correlation surface (computed from implied volatility mid market quotes). Right: daily standard deviation of EUR/JPY-EUR/USD, EUR/JPY-USD/JPY and EUR/USD-USD/JPY implied correlations (based on mid implied volatility market quotes) as a function of option delta and time to maturity.

deviation of implied correlations, as illustrated in the images on the right-hand side of figure 5, again shows surfaces that strongly fluctuate around their average profiles over time. Even though we report a relatively flat term structure for the average correlation surface of each pair, the daily variations of implied correlation values do support the existence of a term structure since shorter-dated implied correlations vary a lot more than longer-dated ones. As in the case of implied volatilities, the smiles' shape change heavily across time.

6. Surface dynamics: volatilities

6.1. Ranked eigenvalues

We begin our analysis by considering the application of the Karhunen-Loève decomposition to the daily logarithmic variations of the implied volatility. We follow Cont and da Fonseca (2002) and rank for each currency pair the obtained absolute eigenvalues f_k in decreasing order. The images on the left-hand side of figure 6 clearly illustrate that the f_k decline rapidly with k . Thus, the variance of daily variations

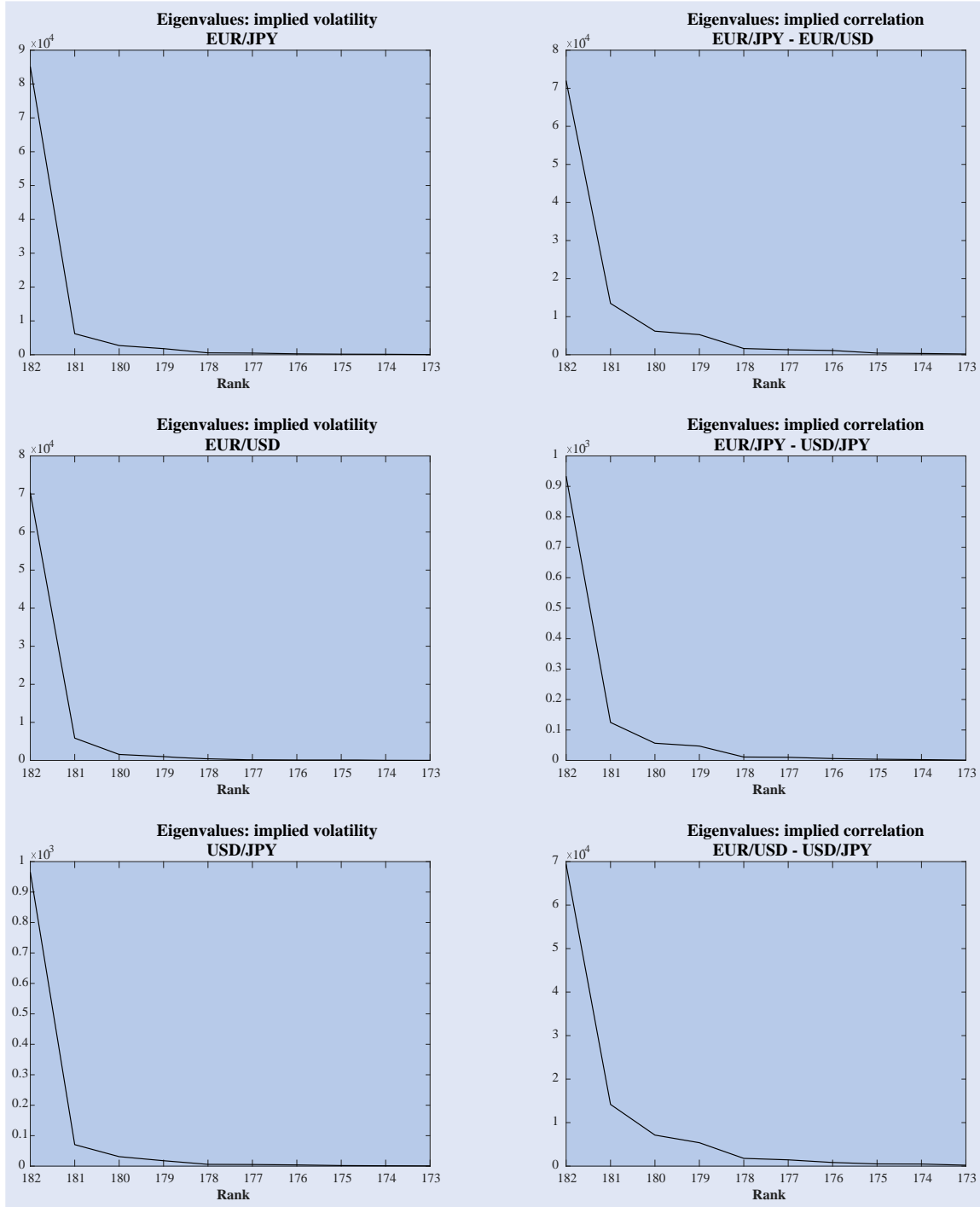


Figure 6. Left: eigenvalues for daily variations in implied volatility surfaces, sorted by their rank. Right: eigenvalues for daily variations in implied correlation surfaces, sorted by their rank.

in implied volatility is best determined by a small number of principal components. To be more precise, the first three eigenmodes explain 96.35% of variance in *EUR/JPY*, 96.61% of variance in *USD/JPY* and 97.62% of variance in *EUR/USD* implied volatility surfaces which is in line with earlier studies (cf., e.g. Skiadopoulos *et al.* 1999, Cont and da Fonseca 2002, Fengler *et al.* 2003 in the equity space). Therefore, we shall solely focus on these first three eigenmodes.

It is certainly far more important, however, that the same first three eigenmodes ('same' in the sense of 'same

eigenmodes' shapes') account for the largest share in variation across all three currency pairs. The only exception is the third eigenmode of the *EUR/USD* surfaces whose shape deviates. The first finding has already been acknowledged by Chalamandaris and Tsekrekos (2010) for a set of 25 different exchange rates, focusing on the time period from 2000 to 2007. But we provide evidence of this to still hold for other currency pairs (and not necessarily with *EUR* as a base currency), and even in a more recent period that additionally includes times of heavy financial turmoil. We will illustrate our results in the following.

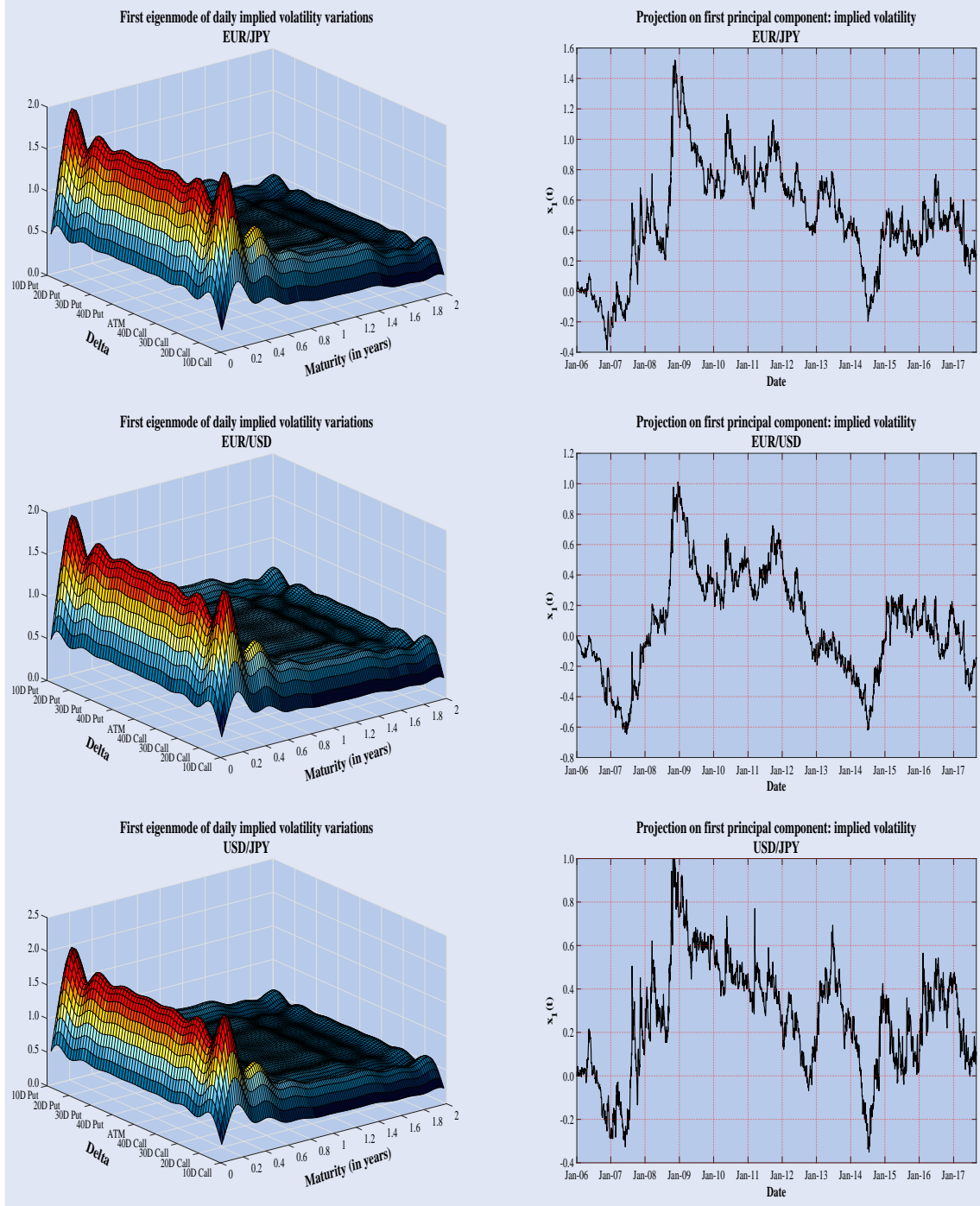


Figure 7. Left: first eigenmode of variations in daily implied volatility surfaces. Right: time evolution of the projection of implied volatilities on the first principal component.

6.2. First eigenmode

We start by discussing the first eigenmode of all three currency pairs *EUR/JPY*, *EUR/USD* and *USD/JPY* in one paragraph since they exhibit remarkable similarities in their shapes. Figure 7 shows the character of these three most dominant eigenmodes that contribute the largest to observed daily variations in implied volatility. The first eigenmode accounts for more than 87% of daily variance in *EUR/JPY*, for roughly 88% of variation in *EUR/USD* and for about 87% of variance given *USD/JPY* implied volatility surfaces. Note that each eigensurface has positive components only. Of particular

interest is the fact that moving towards the option's maturity date results in a positive and sharp increase in value of all components. This is valid for puts and calls likewise, and irrespective of their relative deltas. Thus, there is clear evidence of a steep downward sloping term structure. Shortly before option expiry, however, we observe a sudden drop along the full range of delta values for each option type. Broadly speaking, a positive shock in the direction of the first eigenmode increases all implied volatilities of each currency pair. This trend is intensified with decreasing time to maturity. Ignoring options close to expiry for the moment, the first eigenmode

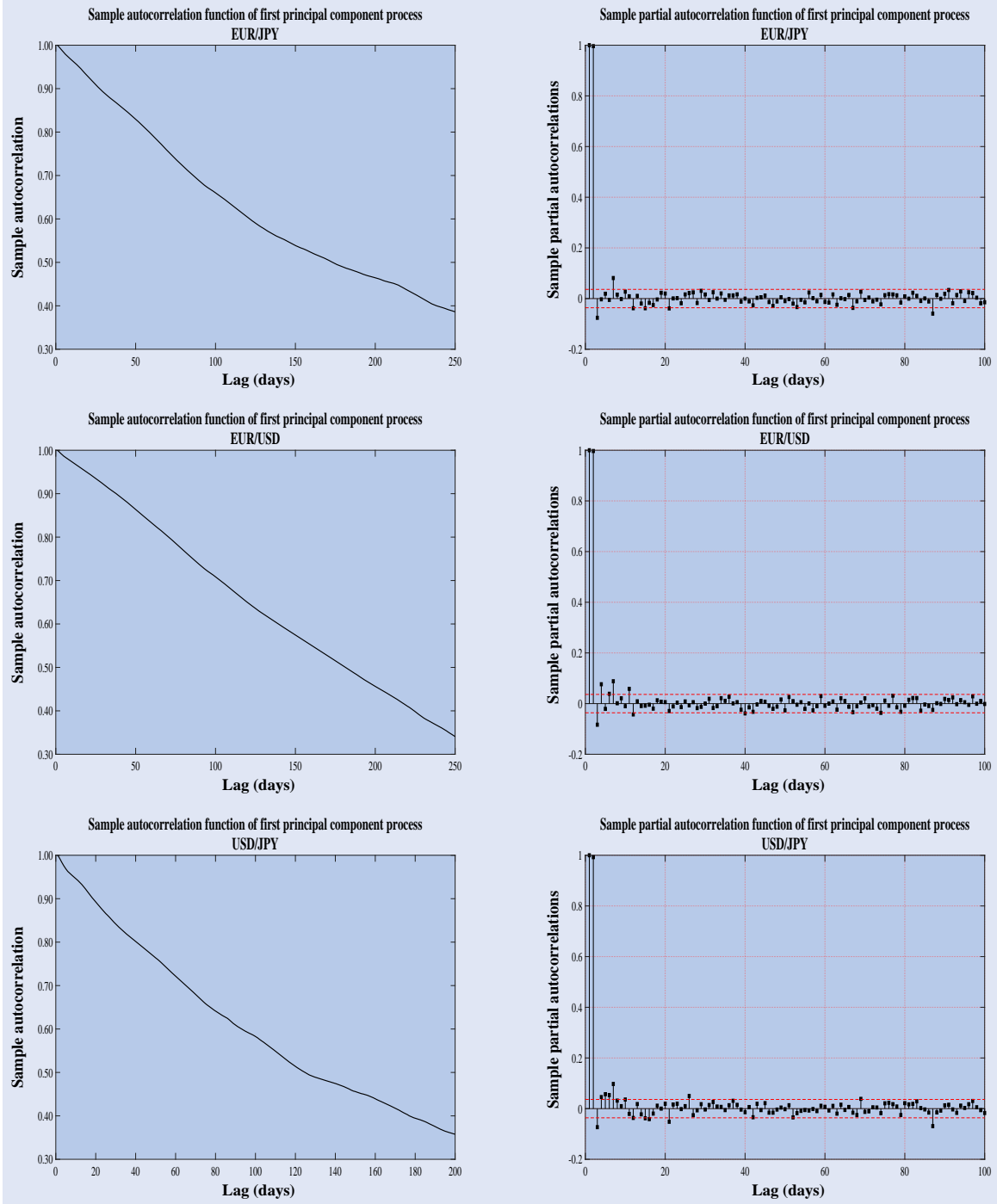


Figure 8. First principal component process, implied volatilities. Left: autocorrelation function of $x_1(t)$. Right: partial autocorrelation coefficients of $x_1(t)$.

may be interpreted as a level effect, combined with a negative term structure factor.

We now consider the projection $x_1(t)$ of daily implied volatility surfaces on this eigenmode. For each exchange rate, there is evidence of a mean reverting behaviour and two large jumps may be observed. While the sudden hike gradually shifts the processes to a new equilibrium, thus persisting over an extended period of time, the unexpected drop is followed by an immediate rise in the processes' values to their pre-shock levels. Figure 1 shows a steady increase in both the *EUR/JPY* and *EUR/USD* exchange rate starting in January

2006, and reaching a peak by the end of July 2008. Following the upward trend, we then observe a sharp decrease (with several up- and downward swings of the market in between) beginning in end-October 2008 and lasting until mid-December of the same year. The identical pattern may be depicted for the *USD/JPY* currency rate, though not as pronounced. This is in line with the movements of each of the three first principal component processes $x_1(t)$. Recall: since all components of the three first eigenmodes are positive, a positive shock increases the particular currency rate's process; a negative shock leads to a decrease.

Table 2. Selected sample autocorrelation coefficients for principal component time series.

Eigenmode	lagged sample autocorrelation coefficients (in days)									
	1-lag	20-lag	50-lag	100-lag	140-lag	200-lag	250-lag	300-lag	350-lag	500-lag
Implied volatility: EUR/JPY										
1	0.996	0.925	0.827	0.658	0.556	0.464	0.385	0.314	0.239	-0.067
2	0.998	0.961	0.902	0.806	0.746	0.659	0.577	0.474	0.377	0.065
3	0.994	0.900	0.786	0.625	0.528	0.417	0.293	0.152	0.042	-0.037
Implied volatility: EUR/USD										
1	0.997	0.946	0.860	0.706	0.596	0.454	0.338	0.203	0.089	-0.123
2	0.997	0.951	0.893	0.808	0.734	0.615	0.504	0.351	0.249	-0.015
3	0.960	0.851	0.775	0.651	0.555	0.442	0.344	0.295	0.246	0.096
Implied volatility: USD/JPY										
1	0.992	0.887	0.760	0.580	0.473	0.356	0.245	0.159	0.089	-0.114
2	0.997	0.949	0.900	0.835	0.790	0.695	0.605	0.499	0.402	0.081
3	0.997	0.941	0.877	0.775	0.695	0.595	0.516	0.441	0.364	0.251

Note: Implied volatility.

For each currency pair, the autocorrelation function of the first principal component process $x_1(t)$ is shown on the left-hand side of figure 8. We observe the autocorrelation coefficients to be significantly[†] positive up to a minimum of 200 days. This corresponds to roughly ten trading months. Table 2 even reports significantly positive values up to more than a trading year. Thus, there is high persistence in the values of the particular first principal component processes. Looking at the partial autocorrelation coefficients (cf. images on the right-hand side of figure 8), we find this persistence to be well approximated by a lower-order autoregressive process. To be more precise, a large portion of the persistence can already be captured by an AR(1) process. The estimation of an AR(1) process[‡] on the three time series results in an autoregression constant of 0.996 for the EUR/JPY, of 0.997 for the EUR/USD, and of 0.993 for the USD/JPY exchange rate. These values give us a corresponding mean reversion speed, or *half-life* (i.e. the time horizon that the process needs (on average) to halve its distance from the mean), of 190.04, 224.35 and 92.65 days, respectively. The average mean reversion time for the first three processes is at least more than three times the period reported for stock indices by Cont and da Fonseca (2002). Compared to stock markets, this implies a far stronger trend following behaviour in currency markets.

6.3. Second eigenmode

We shall now proceed with the second eigenmode. It explains still 6.37% of daily variations in EUR/JPY, 7.36% of variance in EUR/USD and 6.39% of variations in USD/JPY

implied volatility. An interesting point is the striking similarity between the first and second eigenmode's shape across each currency pair, including the remarkable characteristic for options shortly before expiry that leads to the downward sloping term structure feature. Here as well, we observe a strong decline in value of the respective surface's components (cf. first eigenmode). An exception, however, is the fact that only those components that have a time to maturity of less than 0.5 years are positive. The remaining part constituting the majority of the second eigensurface has negative values. This is valid for calls and puts likewise, and given the entire range of delta values each.

The evolution of the projection $x_2(t)$ of daily implied volatility surfaces on the second eigenmode for each of the three currency pairs is shown in figure 9. In light of the aforementioned findings, the occurrence of a positive shock in the direction of this eigenmode leads to a sharp downward movement of all those implied volatilities that are associated with a negative component, while volatilities having a positive component show an increase in value. Since the negative coefficients are in the majority, we observe the principal component process of the second eigenmode $x_2(t)$ to be downward sloping, even though the magnitude in value of the positive coefficients is more pronounced. This is valid for all three exchange rates likewise. To be more precise, the second process may certainly be seen as an almost exact inverse representation of the first principal component process. In line with the first principal component processes, both the spikes and drops for each currency pair are observed to be on the same dates here as well, but the direction has now changed. This means that any previously described rise now turns into a drop, while all declines become spikes. Nevertheless, their economic interpretations is still valid, however vice versa. Moreover, all three time series also show strong indication of an evident mean reverting behaviour, though there is some periodicity in each process.

Investigation of the partial autocorrelation functions of the corresponding second eigenmodes, as illustrated on the right-hand side of figure 10, states the following: again, the correlation structures can be well represented by an AR(1) process. After estimating an AR(1) model on the three time series, we report an autoregression coefficient of 0.998 for the

[†]Please note that the standard error for testing the significance of a single lag-h autocorrelation, $\hat{\rho}_t$, is approximately $SE_{\rho} = (1 + 2 \sum_{i=1}^{h-1} \hat{\rho}_i^2)/N$. In case of sample autocorrelation function plots, approximate 95% confidence intervals are drawn at $\pm 2SE_{\rho}$. In our case, we consider only a limited number of lags such that these bounds are set at a low value. Since they thus do not appear in most of the autocorrelation plots, we decide to suspend them in all charts.

[‡]Table 3 shows that all series of the first two eigenmodes of each currency rate deviate only marginally from normality. Hence, we generally opt for an AR(1) process with Gaussian noise within Section 6.

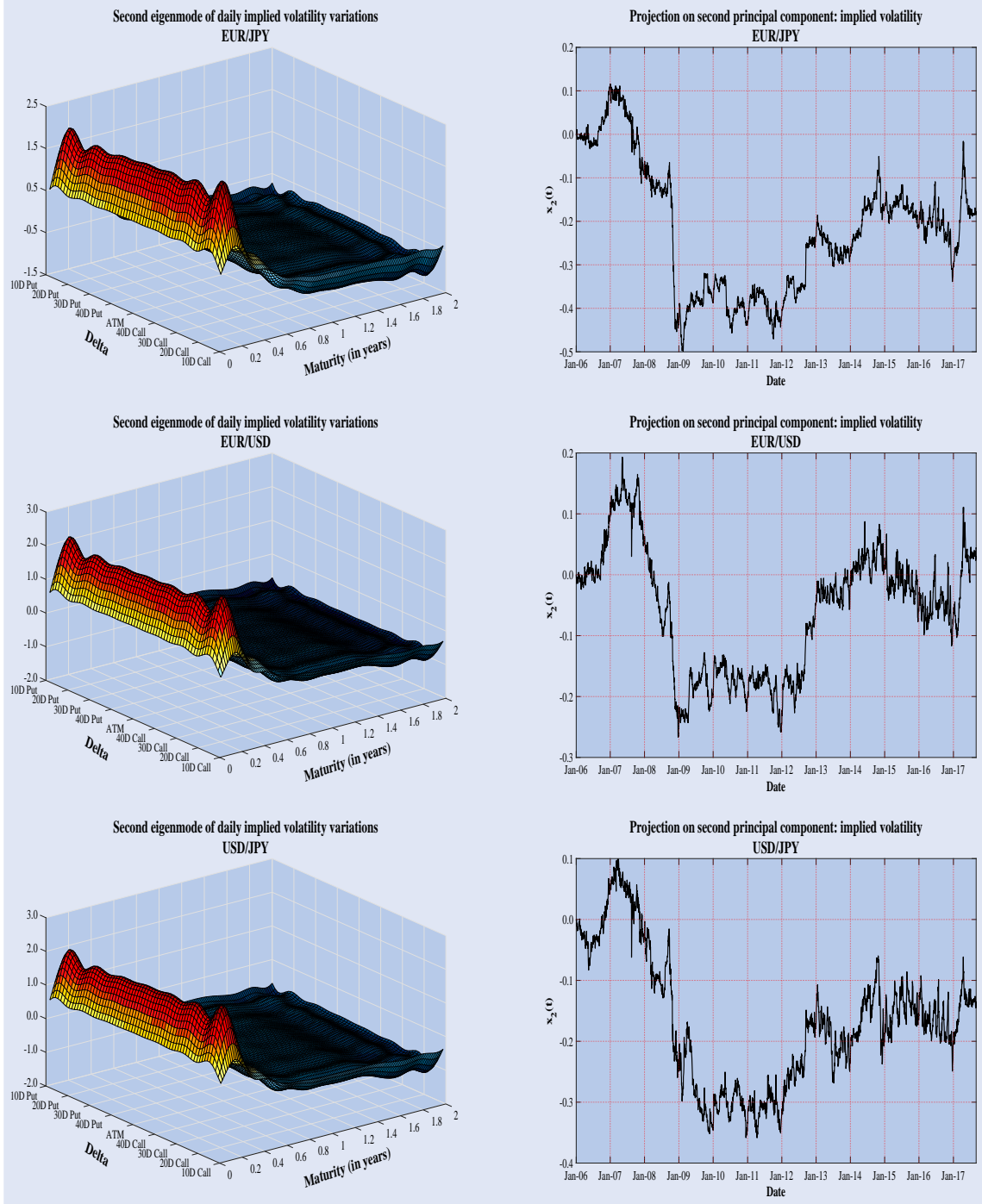


Figure 9. Left: second eigenmode of variations in daily implied volatility surfaces. Right: time evolution of the projection of implied volatilities on the second principal component.

EUR/JPY, of 0.997 for the *EUR/USD*, and of 0.997 for the *USD/JPY* exchange rate. These values imply a corresponding mean reversion speed of 390.53, 252.42 and 209.49 days, respectively.

6.4. Third eigenmode

Lastly, we consider the third eigenmode of each currency pair and start with the *EUR/USD* surface dynamics. Compared to the remaining two currency pairs, the shape of its third eigenmode, as depicted at the centre on the left-hand side

of figure 11, stands out as quite an exemption. It accounts for just 1.97% of daily variation which is the smallest fraction among the presented three third eigenmodes. In addition, the shape itself is quite exceptional and resembles, in a pronounced way, the well-known volatility smile, though not with respect to strike levels (or delta values in our case) but as to time to maturity. Given the full range of deltas, it takes positive values for both calls and puts that are characterized as being either short before expiry or having a remaining maturity of at least 1.6 years. The exception are options on a medium-term basis and independent of the respective delta. These have negative values. To be more precise, the closer

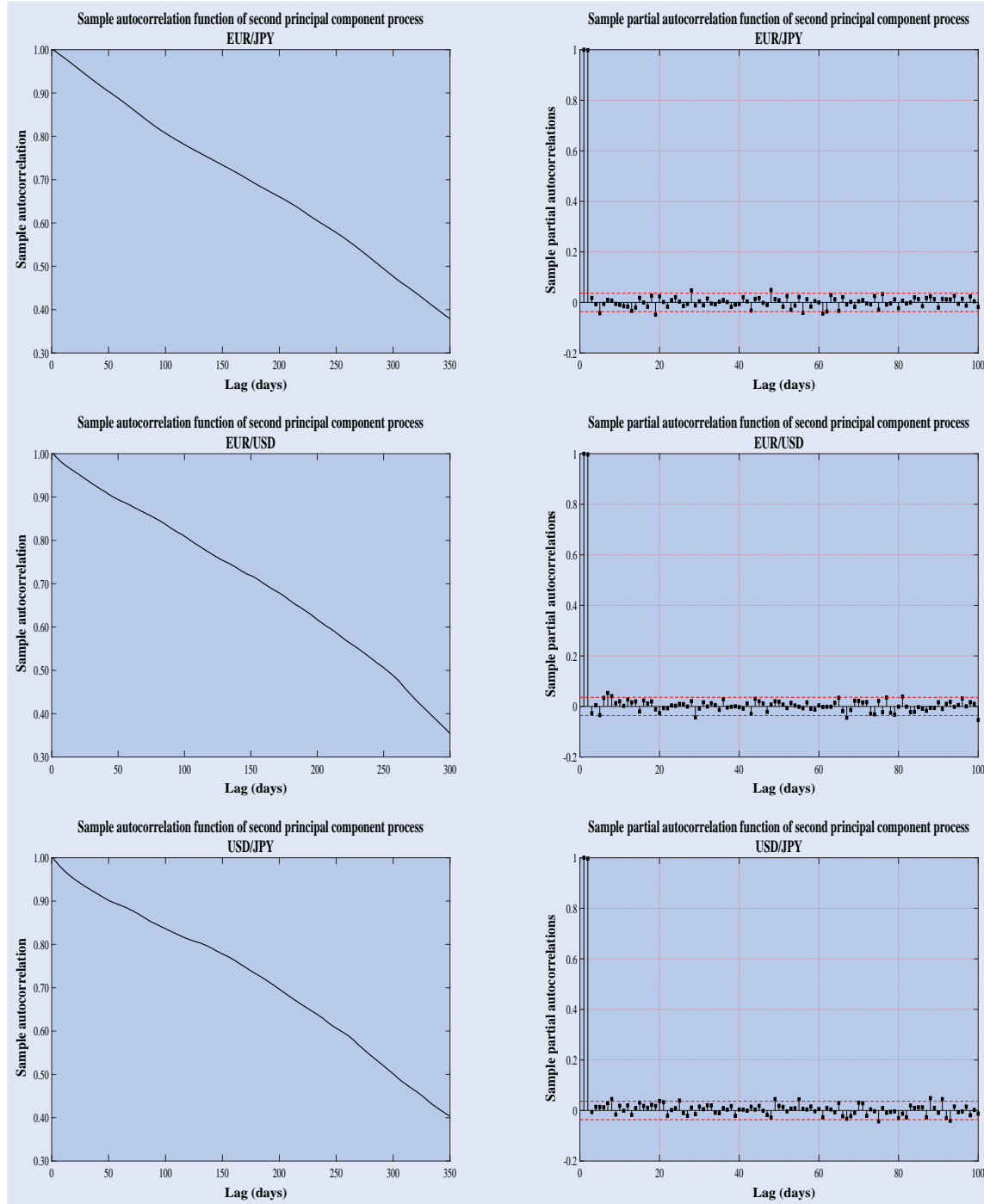


Figure 10. Second principal component process, implied volatilities. Left: autocorrelation function of $x_2(t)$. Right: partial autocorrelation coefficients of $x_2(t)$.

we move to a mid-maturity segment, the more negative the third eigenmode's values become. This is similar to the results reported by Cont and da Fonseca (2002) for S&P 500 options, although the shape of their third eigenmode shows a smile feature along option moneyness which is the common pattern for implied volatilities. They describe this eigenmode as being a butterfly mode and interpret it as a variation in the implied volatility surfaces' convexity. A positive shock within this eigenmode causes the implied volatilities of both calls and puts to increase that are either short- or longer-dated, while implied volatilities of options in the middle term to maturity segment decrease.

The evolution of the projection $x_3(t)$ of daily implied volatility surfaces on the third eigenmode is shown at the centre on the right-hand side of figure 11. Although negative components dominate this eigenmode, the cumulative sum of all positive components' values is of higher magnitude. Thus, we find the process to be upward-sloping for any positive shock in the market. Particularly striking in this respect is the market turmoil during the financial crisis of 2007–2008. We observe three pronounced spikes. Taking into account the previously stated process dynamics, these are in line with the historical EUR/USD exchange rate development depicted in figure 1.

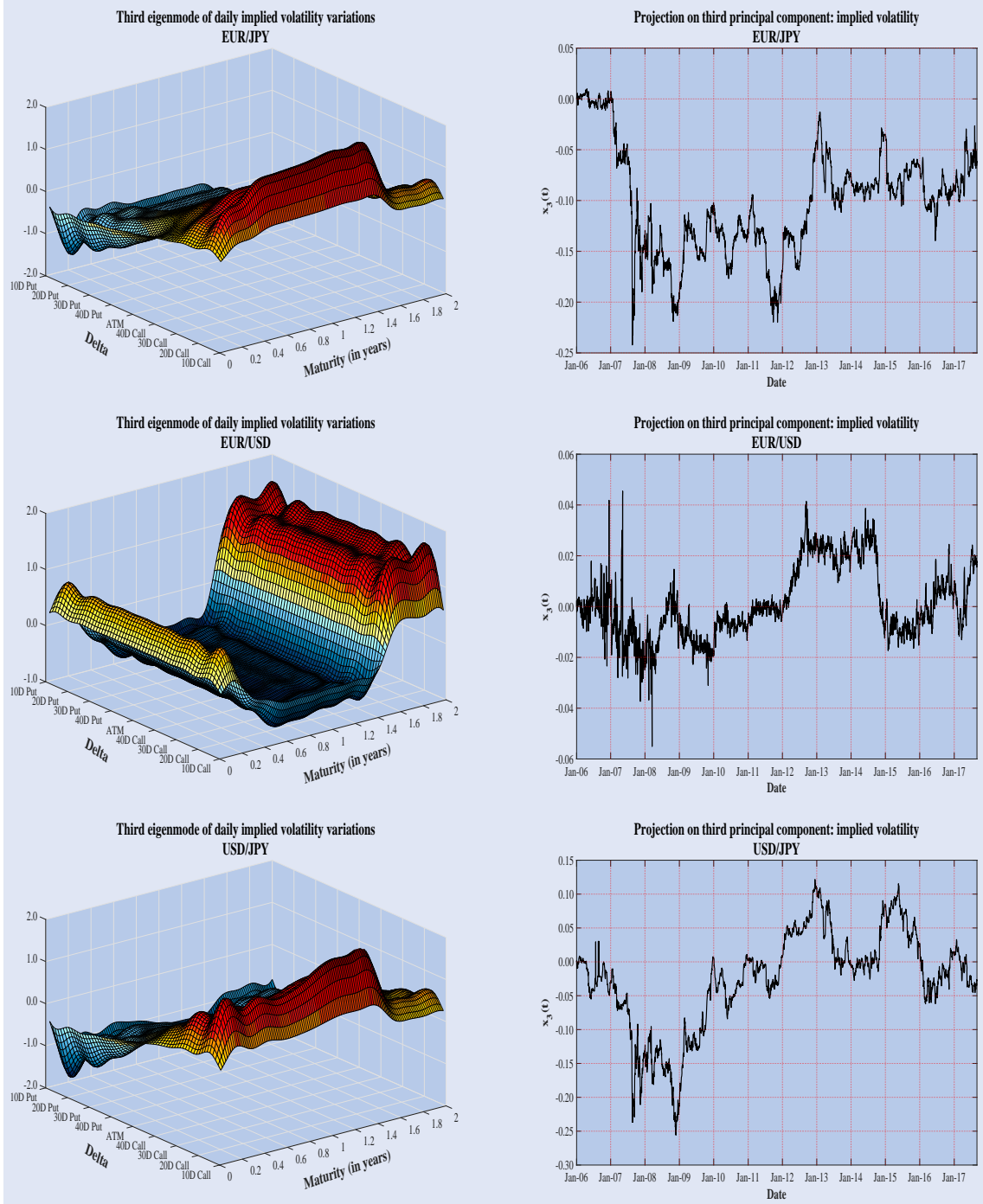


Figure 11. Left: third eigenmode of variations in daily implied volatility surfaces. Right: time evolution of the projection of implied volatilities on the third principal component.

We now turn our attention to the third eigenmode of the remaining two exchange rates *EUR/JPY* and *USD/JPY*; and shall jointly discuss them since they closely resemble each other, both in terms of their relative eigenmode's shapes as well as with respect to the associated principal component processes. The third eigenmode explains 2.78% of variance in *EUR/JPY* and 2.82% of variation in *USD/JPY* implied volatility surfaces. Its relative character is visualized on the top left-hand side and the bottom left-hand side of figure 11, respectively. We observe negative components for out-of-the-money

calls, hence the sign switches at the axis point that indicates at-the-money options. In addition, there is a rise in value when moving along the delta axis, i.e. starting at the outer edge (puts with a delta of 10) and finally approaching calls that have a delta of 10. This pattern clearly exhibits the characteristic feature of a forward skew where, generally speaking, implied volatilities for deep out-of-the-money puts are lower than corresponding implied volatilities for deep out-of-the-money calls. The forward skew pattern common for commodity options indicates a market where there is (fear of) tight supply, hence driving up the demand for out-of-the-money calls

Table 3. Summary statistics for principal component time series.

Eigenmode	Daily standard deviation	Share of variance (in %)	Kurtosis (1 day)	Skewness (1 day)	Mean reversion speed (days)	Correlation with underlying
Implied volatility: EUR/JPY						
1	0.35	87.19	2.90	0.04	190.04	-0.04
2	0.15	6.37	2.26	0.35	390.53	≈ 0
3	0.05	2.78	2.60	0.16	124.74	0.05
Implied volatility: EUR/USD						
1	0.33	88.29	2.68	0.20	224.35	-0.04
2	0.10	7.36	2.10	-0.10	252.42	0.02
3	0.01	1.97	2.48	0.47	17.27	≈ 0
Implied volatility: USD/JPY						
1	0.26	87.40	2.80	≈ 0	92.65	-0.04
2	0.11	6.39	2.42	0.39	209.49	≈ 0
3	0.07	2.82	3.23	-0.65	234.41	0.06

Note: Implied volatility.

Table 4. Proportion of variance (in %) explained by the first three eigenmodes, along with their corresponding shapes.

First eigenmode	Second eigenmode	Third eigenmode
Implied volatility: EUR/JPY		
87.19 (negative term structure and level mode)	6.37 (negative term structure and mixed level mode)	2.78 <small>(forward skew and mixed term structure mode)</small> <small>(convexity mode)</small>
Implied volatility: EUR/USD		
88.29 (negative term structure and level mode)	7.36 (negative term structure and mixed level mode)	1.97 <small>(reversed butterfly mode)</small>
Implied volatility: USD/JPY		
87.40 (negative term structure and level mode)	6.39 (negative term structure and mixed level mode)	2.82 <small>(forward skew and mixed term structure mode)</small> <small>(convexity mode)</small>

Note: Implied volatility.

to secure supply. In addition, we observe a less pronounced upward sloping term structure for calls only, along with a sudden drop in value when considering maturities greater than 1.6 years. Overall, we interpret the third eigenmode as being a convexity factor.

For each currency pair, the projection of implied volatility surfaces on the particular third eigenmode, denoted by $x_3(t)$, is depicted on the top right-hand side and the bottom right-hand side of figure 11, respectively. Both time series are strongly mean reverting and the evolutions over time show signs of pronounced intermittent behaviour. In particular, inspection of the principal component process of EUR/JPY indicates several jumps and spikes, but they match those in the corresponding historical currency rate development.

6.5. Summary statistics

For each of the three currency pairs, table 3 shows summary statistics for the associated time series of the first three principal component processes that are of main interest. The following applies to all processes of each exchange rate: there is high autocorrelation and mean reversion, where the typical mean reversion speed is close to 190 days. The sample

paths are illustrated in figures 7, 9 and 11. After inspecting the partial autocorrelation functions for the first two eigenmodes (as illustrated in figures 8 and 10), we find the autocorrelation structures to be well approximated by AR(1) processes. In addition, we observe excess kurtosis and some skewness such that the unconditional distributions are not of Gaussian type. Nevertheless, all series deviate only marginally from normality. These findings are in line with which is found for S&P 500 and FTSE index options by Cont and da Fonseca (2002).

Particularly striking, however, is the following fact: for each currency pair, all of the first three factors are virtually uncorrelated with the underlying returns. This is contrary to Cont and da Fonseca (2002) who report high correlation values between the underlying returns and the first three factors, whereupon the precise strength and direction depends on the particular factor. Moreover, this finding is inconsistent with the so-called leverage effect observed in the equity space, where implied volatility and asset returns are generally negatively correlated.

Table 4 summarizes the proportion of variance (in %) that is explained by each of the first three principal components, along with the characteristics of each eigenmode.

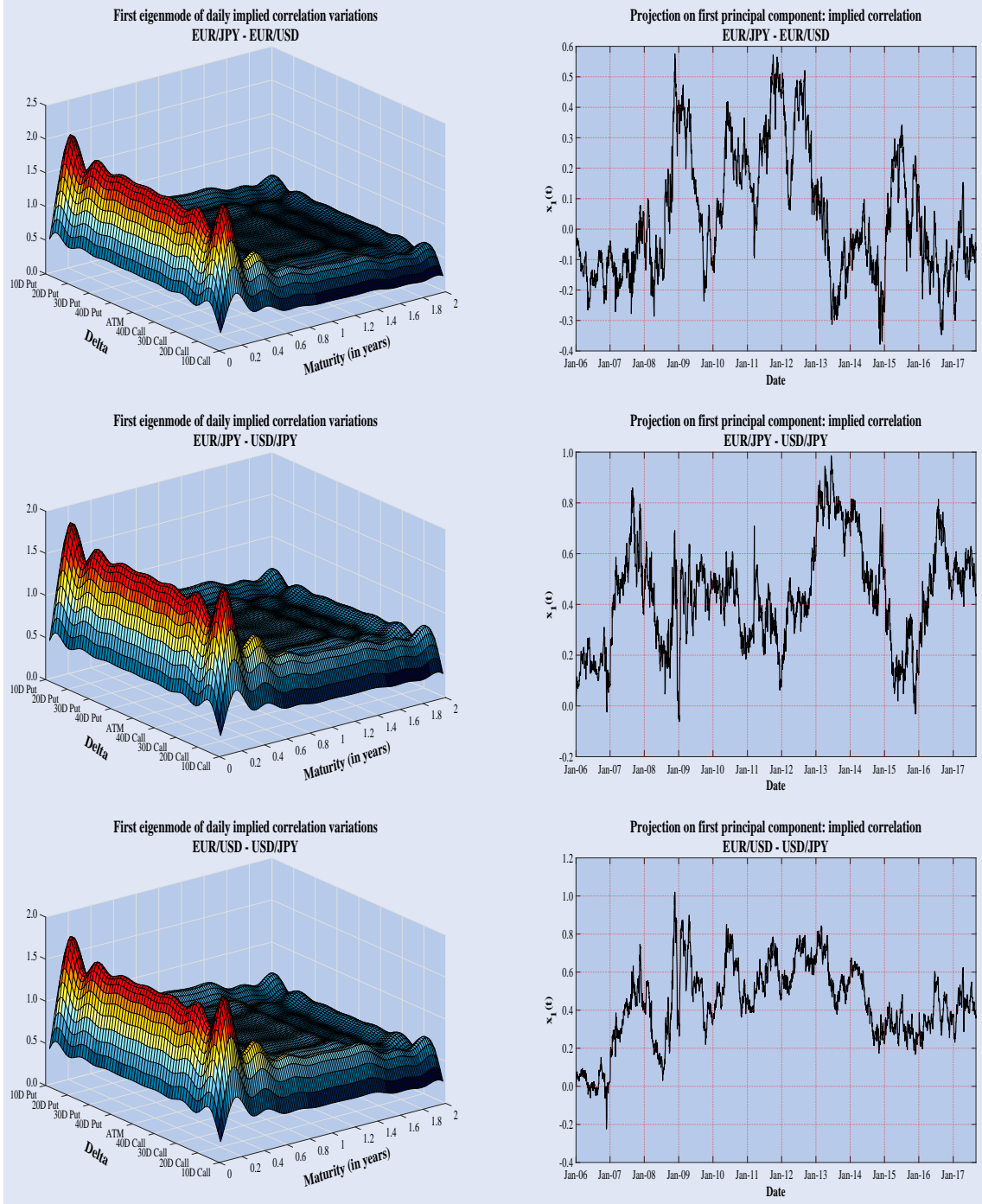


Figure 12. Left: first eigenmode of variations in daily implied correlation surfaces. Right: time evolution of the projection of implied correlations on the first principal component.

7. Surface dynamics: correlations

7.1. Ranked eigenvalues

We subsequently analyse the application of the Karhunen-Loëve decomposition to the daily inverse hyperbolic tangent variations of the implied correlation. We again follow Cont and da Fonseca (2002) and firstly rank for each correlation pair the obtained absolute eigenvalues f_k in decreasing order. Here as well, the images on the right-hand side of figure 6 clearly illustrate that the f_k decline rapidly with k . The variance of daily variations in implied correlation is thus

best determined by a small number of principal components. That is to say: the first three eigenmodes explain 89.70% of variance in EUR/JPY-EUR/USD, 92.97% of variance in EUR/JPY-USD/JPY and 89.27% of variance in EUR/USD-USD/JPY implied correlation surfaces. As a result, we solely consider the first three eigenmodes. Recalling the findings of Section 6, we again observe the same first three eigenmodes to account for the largest share in variation across all three correlation pairs. In addition, these three eigenmodes are identical to those depicted for implied volatility. This will be presented in detail below.

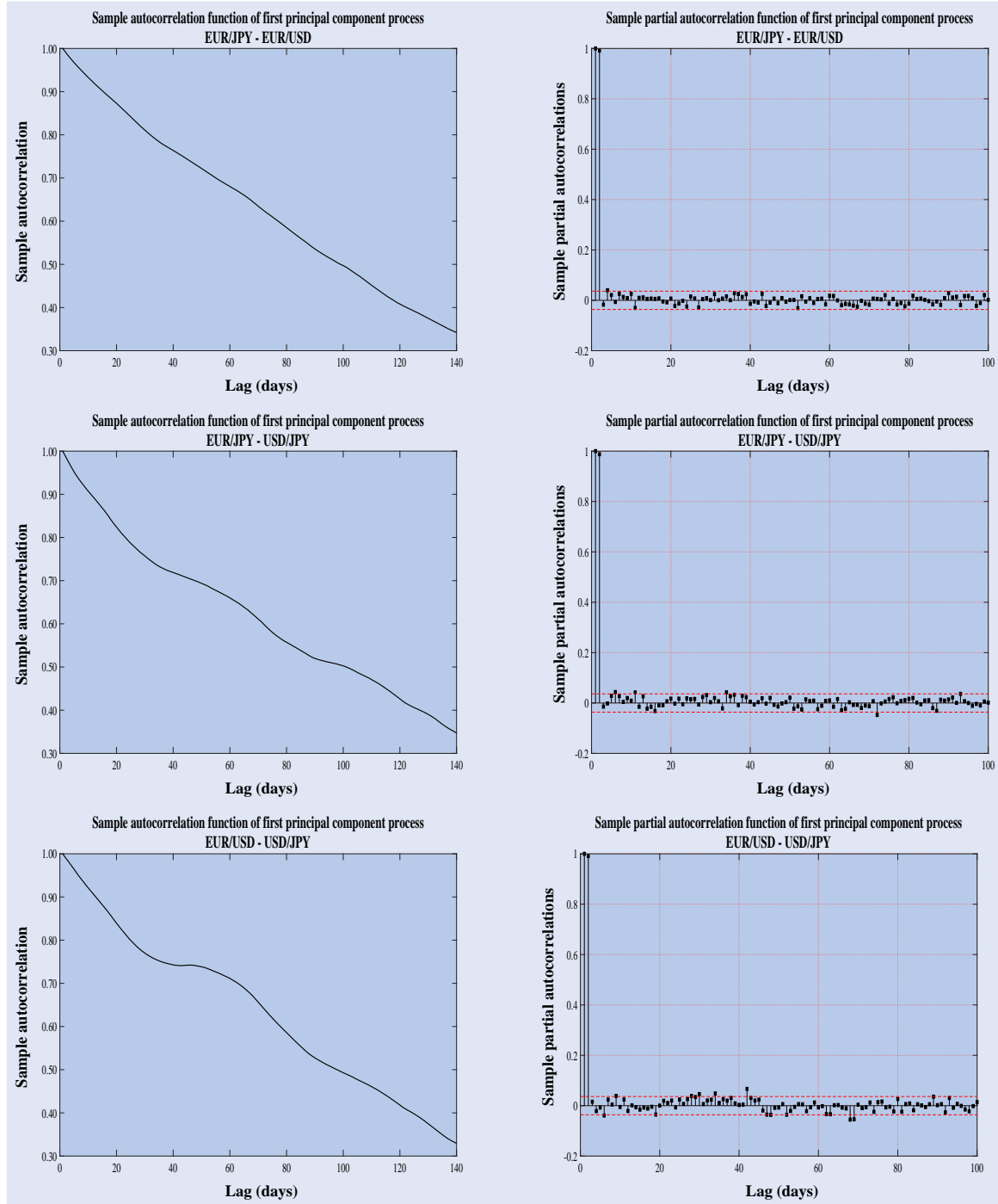


Figure 13. First principal component process, implied correlations. Left: autocorrelation function of $x_1(t)$. Right: partial autocorrelation coefficients of $x_1(t)$.

Given the correlation pairs *EUR/JPY-EUR/USD*, *EUR/JPY-USD/JPY* and *EUR/USD-USD/JPY*, we shall discuss their first three eigenmodes each in one paragraph since they exhibit striking similarities in their shapes. In this regard, it is also worth mentioning that the first three eigenmodes of each pair closely resemble those of both *EUR/JPY* and *USD/JPY*. Consequently, the analysis of their shapes' characteristics is mostly in line with what has already been reported in case of implied volatility (cf. Section 6).

7.2. First eigenmode

To begin with, we consider the first eigenmode of each pair. Figure 12 shows the shape of those three eigensurfaces that account for the largest share in observed daily variations in implied correlation, i.e. the first eigenmode explains more than 70% of daily variance in *EUR/JPY-EUR/USD*, about 78% of variation in *EUR/JPY-USD/JPY* and roughly 68% of variance in *EUR/USD-USD/JPY* implied correlation. For

Table 5. Selected sample autocorrelation coefficients for principal component time series.

Eigenmode	lagged sample autocorrelation coefficients (in days)									
	1-lag	20-lag	50-lag	100-lag	140-lag	200-lag	250-lag	300-lag	350-lag	500-lag
Implied correlation: EUR/JPY-EUR/USD										
1	0.992	0.867	0.718	0.494	0.339	0.206	0.186	0.166	0.160	-0.102
2	0.984	0.835	0.686	0.441	0.277	0.166	0.165	0.117	0.113	-0.104
3	0.996	0.951	0.910	0.840	0.777	0.686	0.625	0.578	0.542	0.426
Implied correlation: EUR/JPY-USD/JPY										
1	0.988	0.816	0.691	0.500	0.342	0.119	-0.076	-0.256	-0.341	-0.247
2	0.988	0.860	0.797	0.690	0.635	0.498	0.433	0.379	0.327	0.286
3	0.995	0.938	0.884	0.815	0.766	0.713	0.653	0.609	0.558	0.443
Implied correlation: EUR/USD-USD/JPY										
1	0.991	0.831	0.737	0.490	0.326	0.261	0.240	0.262	0.272	0.022
2	0.985	0.845	0.714	0.516	0.409	0.327	0.357	0.359	0.338	0.112
3	0.965	0.814	0.711	0.631	0.522	0.384	0.268	0.133	0.073	-0.050

Note: Implied correlation.

Table 6. Summary statistics for principal component time series.

Eigenmode	Daily standard deviation	Share of variance (in %)	Kurtosis (1 day)	Skewness (1 day)	Mean reversion speed (days)
Implied correlation: EUR/JPY-EUR/USD					
1	0.21	70.45	2.37	0.56	82.80
2	0.07	13.30	5.17	-1.09	45.05
3	0.09	6.05	1.96	0.24	169.16
Implied correlation: EUR/JPY-USD/JPY					
1	0.20	77.86	2.49	0.11	57.23
2	0.08	10.41	2.70	0.68	61.31
3	0.08	4.71	2.58	-0.54	142.12
Implied correlation: EUR/USD-USD/JPY					
1	0.20	68.28	2.75	-0.28	77.20
2	0.07	13.96	2.63	0.44	47.15
3	0.03	7.02	2.61	-0.07	19.95

Note: Implied correlation.

each eigensurface, we exclusively observe positive components. Thus, a positive shock in the direction of this eigenmode leads to a rise in all implied correlations. This trend is stronger, the larger the components' magnitude. Moreover, we find the components to increase in value with decreasing time to maturity. They thus show clear signs of a steep downward-sloping term structure. With options close to expiry being elided, we may characterize the first eigenmode as being a level factor, along with a negative term structure effect. This applies to all three correlation pairs likewise.

The projection $x_1(t)$ of the daily implied correlation surfaces on the particular pair's first eigenmode exhibits strongly persistent mean reverting behaviour. Its evolution over time is characterized by a distinct degree of periodicity. For each process, we find several pronounced peaks and drops which are in line with corresponding up- and downward movements in those currency rate pairs forming the respective implied correlation of interest.

For each correlation pair, the autocorrelation function of the first principal component process $x_1(t)$ is shown on the left-hand side of figure 13. The autocorrelation coefficients are significantly positive up to a minimum of 140 days, translating into roughly seven trading months. Table 5 confirms them

to be significantly positive up to more than a trading year. Again, we find high persistence in the values of the particular first principal component processes. Looking at the partial autocorrelation functions (cf. images on the right-hand side of figure 8), the one-day lagged partial autocorrelation coefficients are significant and fall to insignificant levels after one day. This is valid for all three correlation pairs. Here as well, we thus opt for an AR(1) correlation structure.[†] The estimation of an AR(1) process on the three time series results in an autoregression constant of 0.992 for the EUR/JPY-EUR/USD, of 0.988 for the EUR/JPY-USD/JPY, and of 0.991 for the EUR/USD-USD/JPY implied correlation. These values imply a corresponding mean reversion speed of 82.80, 57.23 and 77.20 days, respectively. Please note that this is far below the above reported average speed of approximately 190 days for implied volatility (cf. table 2).

[†] Since table 6 confirms that all series of the first two eigenmodes of each correlation pair deviate only marginally from normality, we generally select an AR(1) process with Gaussian noise within Section 7. However, an exception is the second principal component process of EUR/JPY-EUR/USD for which we decide to estimate an AR(1) process with non-Gaussian noise. To be more precise, a double-exponentially distributed noise is chosen.

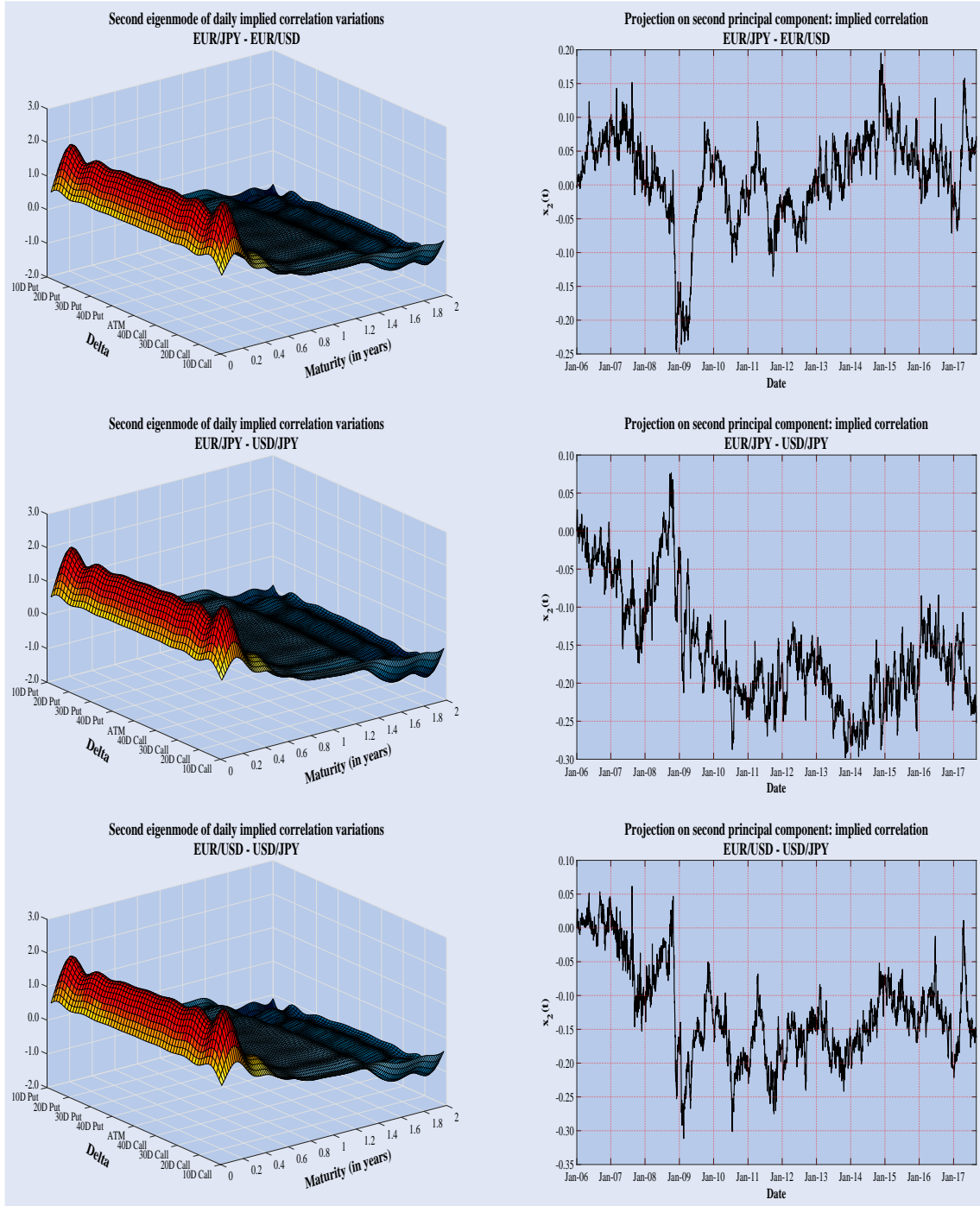


Figure 14. Left: second eigenmode of variations in daily implied correlation surfaces. Right: time evolution of the projection of implied correlations on the second principal component.

7.3. Second eigenmode

We now proceed with the second eigenmode, as shown in figure 14. It accounts for 13.20% of variations in *EUR/JPY-EUR/USD*, for 10.41% of variance in *EUR/JPY-USD/JPY* and for 13.96% of variations in *EUR/USD-USD/JPY* daily implied correlation surfaces. For each pair, the shape of the first and second eigenmode is almost identical such that the previously described level and downward-sloping term structure feature is valid here as well. In line with the implied

volatility case, only those components of the second eigenmode's surface that are associated with a time to maturity of less than 0.5 years are positive, while the remaining majoritarian part has negative values. This applies to both puts and calls, irrespective of their relative delta values. To conclude, we confirm these results to hold for all three correlation pairs likewise.

Next, the projection $x_2(t)$ of the implied correlation surfaces on the second eigenmode is examined. Given the aforementioned findings, a positive shock in the direction of the

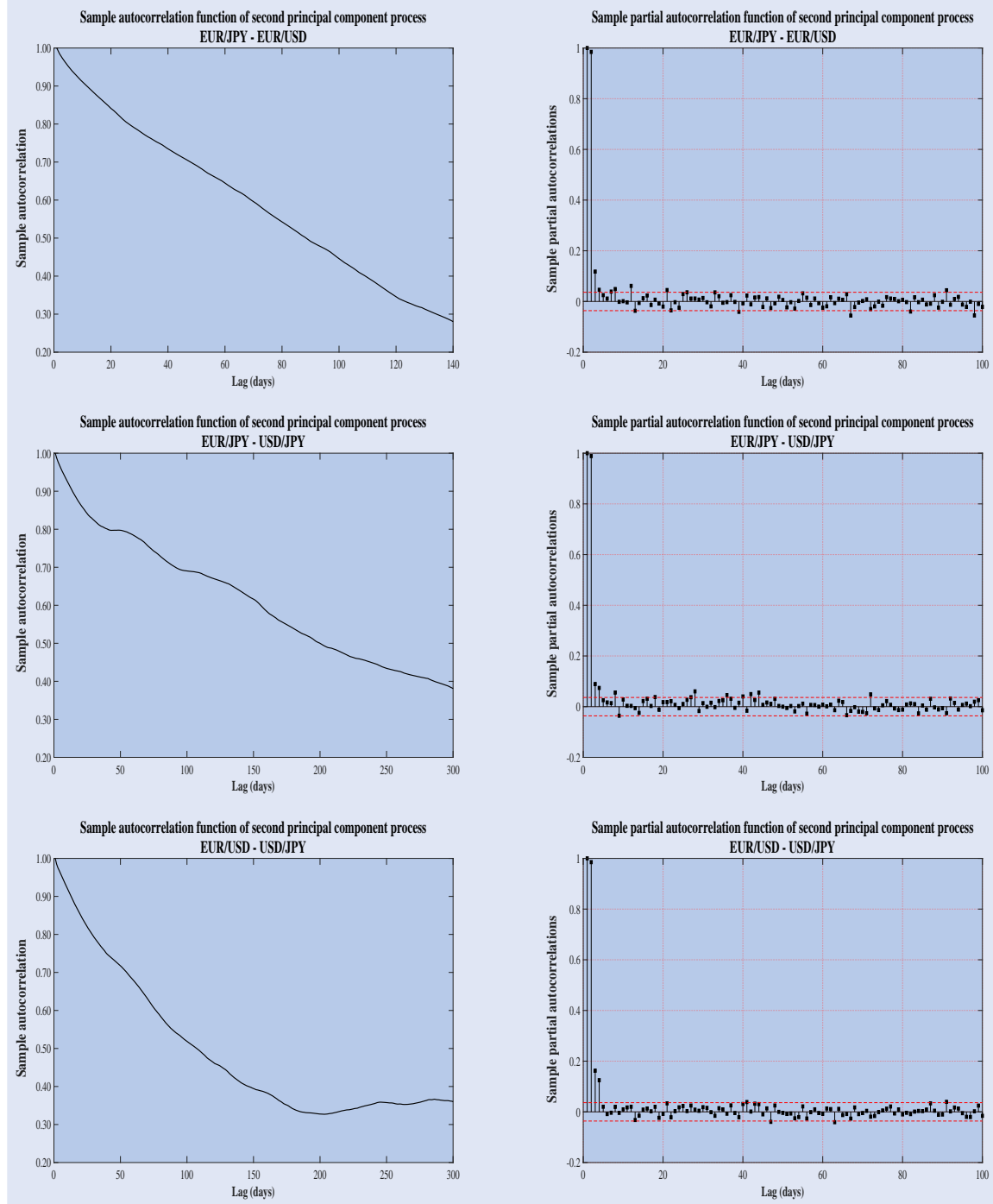


Figure 15. Second principal component process, implied correlations. Left: autocorrelation function of $x_2(t)$. Right: partial autocorrelation coefficients of $x_2(t)$.

second eigenmode decreases all those implied correlation values that have negative components and simultaneously increase implied correlation being associated with positive components. Since the negative components are in the majority, the principal component process is found to be downward-sloping for any positive market shock. All three time series show strong indication of mean reversion. We observe one pronounced drop prior to year-end of 2008 for *EUR/JPY-EUR/USD* and *EUR/USD-USD/JPY*, respectively. In addition, there is one large spike at the beginning of October 2008 for the *EUR/JPY-USD/JPY* correlation pair. Note that each spike and drop is in line with the joint development of any two of the

three exchange rates that are shown in figure 1, thus having a distinct economic justification.

The particular partial autocorrelation functions of all three second eigenmodes are depicted on the right-hand side of figure 10. The implication is as follows: we are able to well approximate the correlation structure by an AR(1) process. After estimating an AR(1) model on the three time series, we report an autoregression coefficient of 0.985 for the *EUR/JPY-EUR/USD*, of 0.989 for the *EUR/JPY-USD/JPY*, and of 0.985 for the *EUR/USD-USD/JPY* implied correlation. These values correspond to a mean reversion speed of 45.05, 61.31 and 47.15 days, respectively.

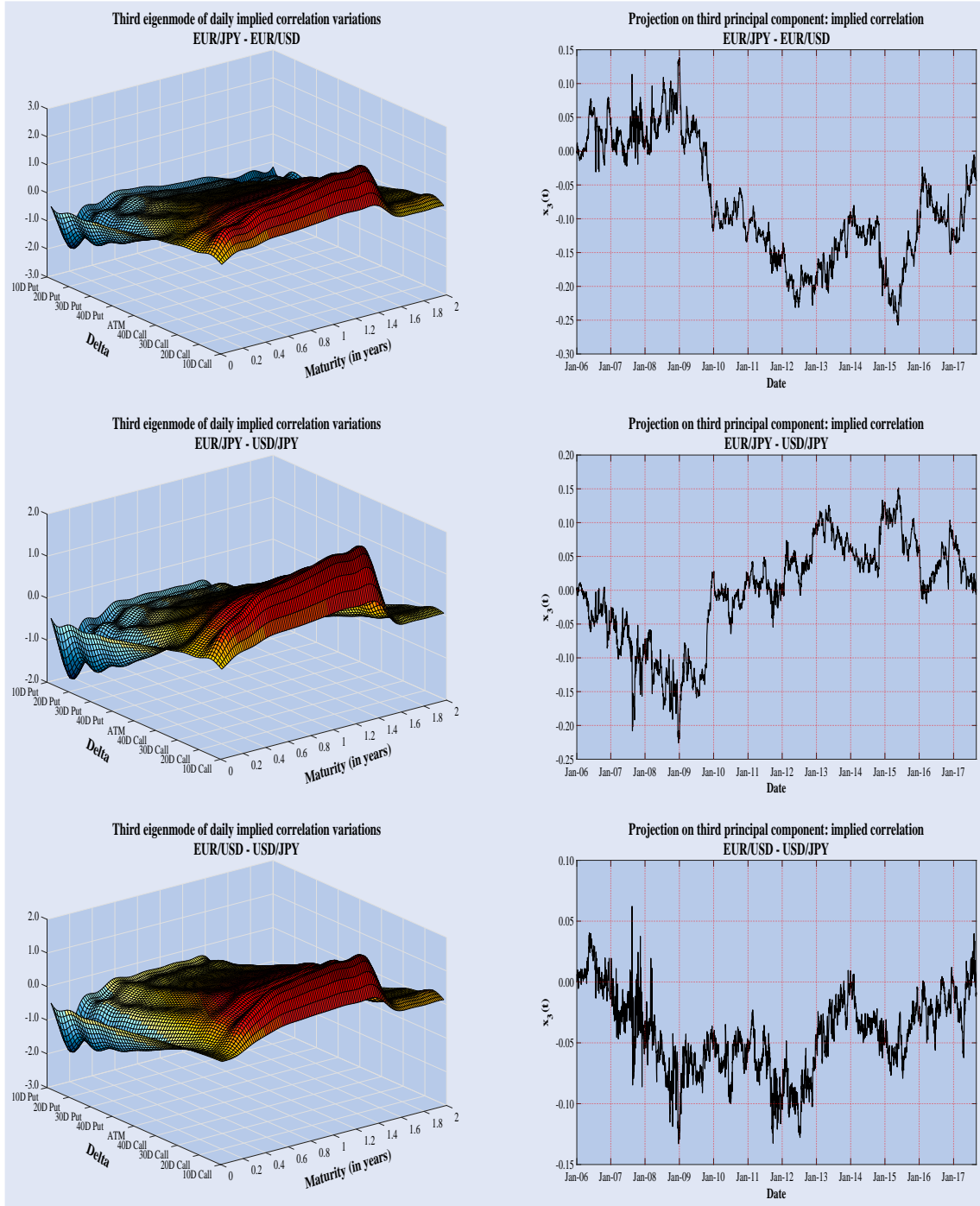


Figure 16. Left: third eigenmode of variations in daily implied correlation surfaces. Right: time evolution of the projection of implied correlations on the third principal component.

7.4. Third eigenmode

Lastly, we shall consider the third eigenmode of each correlation pair, as depicted in figure 16. It adds 6.05% to daily variation in EUR/JPY-EUR/USD, 4.71% to variation in EUR/JPY-USD/JPY and 7.02% to variation in EUR/USD-USD/JPY implied correlation surfaces. As already indicated for implied volatility, we clearly observe the existence of a forward skew. To be more precise, while deep out-of-the-money puts have negative components and thus exhibit a decrease in correlation values for any positive shock in the market, deep out-of-the-money calls show positive components and hence

an increase in correlation. Additionally, with respect to calls, there is some evidence of a less pronounced upward-sloping term structure, along with a sudden drop in those values associated with maturities above 1.6 years. In summary, the third eigenmode may again be interpreted as a convexity effect.

We finally examine the third principal component process, $x_3(t)$, of the three correlation pairs. Since we once again find the negative components to be in the majority, although merely marginal, $x_3(t)$ is downward-sloping for any positive shock that occurs in the market. Of particular interest is the market turmoil during the 2007–2008 financial crisis and its impact at the beginning of the year 2009. There

Table 7. Proportion of variance (in %) explained by the first three eigenmodes, along with their corresponding shapes.

First eigenmode	Second eigenmode	Third eigenmode
Implied correlation: EUR/JPY-EUR/USD 70.45 (negative term structure and level mode)	13.20 (negative term structure and mixed level mode)	6.05 forward skew and mixed term structure mode (convexity mode)
Implied correlation: EUR/JPY-USD/JPY 77.86 (negative term structure and level mode)	10.41 (negative term structure and mixed level mode)	4.71 forward skew and mixed term structure mode (convexity mode)
Implied correlation: EUR/USD-USD/JPY 68.28 (negative term structure and level mode)	13.96 (negative term structure and mixed level mode)	7.02 forward skew and mixed term structure mode (convexity mode)

Note: Implied correlation.

are two to three pronounced spikes in each process, i.e. two upward-pointing peaks for the *EUR/JPY-EUR/USD* correlation pair, three upward-pointing peaks for the *EUR/USD-USD/JPY* pair and two downward-pointing peaks for the *EUR/JPY-USD/JPY* pair. These movements are in line with observed historical developments of those exchange rate pairs that constitute the respective correlation of interest (cf. figure 1). The aforementioned spikes for *EUR/JPY-EUR/USD* and *EUR/USD-USD/JPY*, respectively, are associated with common declines in both the *EUR/JPY* and the *EUR/USD* exchange rate during 2007–2008. The drops for *EUR/JPY-USD/JPY* are related to common rises of the two exchange rates forming this correlation pair.

7.5. Summary statistics

For each of the three correlation pairs, table 6 shows summary statistics for the corresponding time series of the first three principal component processes that are of main interest.[†] The sample paths are depicted in figures 12, 14 and 16. In line with implied volatility, the following applies to all processes of each pair: we observe high autocorrelation and mean reversion, and the correlation structure is well approximated by an AR(1) process that has an average mean reversion speed of roughly 87 days, being less than half the speed reported for the implied volatility case (cf. partial autocorrelation functions that are illustrated in figures 13 and 15). In addition, we find excess kurtosis and some skewness such that the unconditional distributions are not of Gaussian type. Nevertheless, all series deviate only marginally from normality. An exception, however, is the second eigenmode's process of *EUR/JPY-EUR/USD*. It has significant non-Gaussian features, pointing to the application of an AR(1) model with non-Gaussian noise.

Table 7 summarizes the proportion of variance (in %) that is explained by each of the first three principal components, along with the characteristics of each eigenmode.

[†] Unlike implied volatilities, we are unable to compute the correlation between the first three factors and the underlying returns. The reason for this is simple: implied correlation refers to a set of two underlyings, and thus two return series.

8. Conclusion

We collect historical implied volatility quotes for the three currency pairs *EUR/JPY*, *EUR/USD* and *USD/JPY*, given a range of delta values and time to maturities. The period under investigation ranges from January 4th, 2006 to September 1st, 2017, covering 3,041 trading days. In addition, we consider historical implied correlation between the three currency pairs introduced above. Implied correlation is computed using implied volatilities.

To begin with, we construct daily smooth implied volatility and implied correlation surfaces, respectively, using a two-dimensional kernel smoothing technique. In detail, we employ a non-parametric Nadaraya-Watson estimator with a Gaussian kernel that yields a time series of smooth surfaces. Next, we compute daily variations of the natural logarithm of implied volatility and daily variations of the inverse hyperbolic tangent of implied correlation to which we then apply a Karhunen-Loëve decomposition. The approach is a generalization of the principal component analysis to investigate the dynamics of higher dimensional data, i.e. surfaces, over time.

The statistical analysis of the two surface types reveals the following results:

- (i) The largest share in daily variations in the natural logarithm of implied volatility is determined by identical first three principal components across all three currency pairs. Given the three correlation pairs, the same applies to daily variations in the inverse hyperbolic tangent of implied correlation.
- (ii) The identical first three eigenmodes account for the largest share in daily variations for both implied volatility and implied correlation. This confirms the existence of a strong dependence structure between both concepts.
- (iii) These findings even hold under different market regimes.
- (iv) The first eigenmode may be interpreted as a level effect, combined with a negative term structure factor.
- (v) The second eigenmode reflects the interaction between a negative term structure effect and a mixed level effect.

- (vi) The third eigenmode may be characterized as a forward skew factor combined with a mixed term structure effect. Overall, we call it a convexity effect.
- (vii) Movements in implied volatility are virtually uncorrelated with movements in the underlying asset.
- (viii) The projections of implied volatility surfaces on the particular first three eigenmodes (principal component processes) show highly and primarily positive autocorrelation. In addition, a pronounced mean-reverting behaviour is observed. These characteristics are also valid for the projections of implied correlation surfaces on their eigenmodes.
- (ix) The autocorrelation structure of all principal component processes for both implied volatility and implied correlation is well approximated by an AR(1) process.

To conclude, we provide an important contribution to the pricing of both more complex and multi-asset options. Additionally, our findings may also be applied in the area of constructing hedging strategies for portfolios if one is exposed to currency risk, for example. In each case, the consideration of entire surfaces is required. The sole application of implied at-the-money volatility (and correlation likewise) generates insufficient results. Since these surfaces' movements capture the evolution of option prices, it is thus of high importance for market participants to have a profound knowledge on their dynamics.

Disclosure statement

No potential conflict of interest was reported by the authors.

References

- Ahmed, J. and Straetmans, S., Predicting exchange rate cycles utilizing risk factors. *J. Empirical Financ.*, 2015, **34**, 112–130.
- Alexander, C., Principal component analysis of implied volatility smiles and skews. ISMA Centre Discussion Papers in Finance, University of Reading, 2001.
- Alexander, C. and Kaeck, A., Volatility dynamics for the S&P 500: Further evidence from non-affine, multi-factor jump diffusions. *J. Bank. Financ.*, 2012, **36**, 3110–3121.
- Anatolyev, S., Gospodinov, N., Jamali, I. and Liu, X., Foreign exchange predictability and the carry trade: A decomposition approach. *J. Empirical Financ.*, 2017, **42**, 199–211.
- Bernales, A. and Guidolin, M., Can we forecast the implied volatility surface dynamics of equity options? Predictability and economic value tests. *J. Bank. Financ.*, 2014, **46**, 326–342.
- Bisesti, L., Castagna, A. and Mercurio, F., Consistent pricing and hedging of an FX options book. *Kyoto Econ. Rev.*, 2005, **74**(1), 65–83.
- Bloomberg, FX volatility surface interpolation/extrapolation FAQ. Quantitative Research and Development FX Team, 2009.
- Bodurtha, J.N. and Shen, Q., *Historical and Implied Measures of 'Value at Risk': The DM and Yen Case*, 1995 (Georgetown University: Washington, DC).
- Brockmann, M., Gasser, T. and Hermann, E., Locally adaptive bandwidth choice for kernel regression estimators. *J. Am. Stat. Assoc.*, 1993, **88**(424), 1302–1309.
- Butler, C. and Cooper, N., Implied exchange rate correlations and market perceptions of European Monetary Union. Bank of England Quarterly Bulletin, 1997.
- Campa, J.M. and Chang, P.H.K., The forecasting ability of correlations implied in foreign exchange options. *J. Int. Money Financ.*, 1998, **17**(6), 855–880.
- Cassese, G. and Guidolin, M., Modelling the MIB30 implied volatility surface: Does market efficiency matter? Working Paper 2005-008A, Federal Reserve Bank of St. Louis, 2005.
- CBOE, CBOE S&P 500 implied correlation index [online]. Available online at: <https://www.cboe.com/micro/impliedcorrelation/ImpliedCorrelationIndicator.pdf> (accessed 20 December 2017).
- Cenedese, G., Sarno, L. and Tsakas, I., Foreign exchange risk and the predictability of carry trade returns. *J. Bank. Financ.*, 2014, **42**, 302–313.
- Chalamandaris, G. and Tsekrekos, A.E., Predictable dynamics in implied volatility surfaces from OTC currency options. *J. Bank. Financ.*, 2010, **34**, 1175–1188.
- Christensen, B.J. and Prabhala, N.R., The relation between implied and realized volatility. *J. Financ. Econ.*, 1998, **50**(2), 125–150.
- Clemens, A.E., Hurn, A.S. and Volkov, V.V., Volatility transmission in global financial markets. *J. Empir. Financ.*, 2015, **32**, 3–18.
- Cont, R. and da Fonseca, J., Dynamics of implied volatility surfaces. *Quant. Finance*, 2002, **2**(1), 45–60.
- Cooper, N. and Talbot, J., The yen/dollar exchange rate in 1998: Views from the options markets. Bank of England Quarterly Bulletin, England, 1999.
- Della, Corte and Tsakas, I., Spot and forward volatility in foreign exchange. *J. Financ. Econ.*, 2011, **100**(3), 496–513.
- Dempsey, M. and Tanha, H., The evolving dynamics of the Australian SPI 200 implied volatility surface. *J. Int. Financ. Markets Inst. Money*, 2016, **43**, 44–57.
- Dijk, V.D., Opschoor, A. and van der Wel, M., Predicting volatility and correlations with financial conditions indexes. *J. Empir. Financ.*, 2014, **29**, 435–447.
- Egbers, T. and Swinkels, L., Can implied volatility predict returns on the currency carry trade? *J. Bank. Financ.*, 2015, **59**, 14–26.
- Fengler, M.R., Härdle, W. and Schmidt, P., Common factors governing VDAX movements and the maximum loss. *Financ. Market Portfolio Manage.*, 2002, **16**(1), 16–29.
- Fengler, M.R., Härdle, W. and Villa, C., The dynamics of implied volatilities: A common principal components approach. *Rev. Deriv. Res.*, 2003, **6**, 179–202.
- Fernandes, M., Medeiros, M.C. and Scharth, M., Modelling and predicting the CBOE market volatility index. *J. Bank. Financ.*, 2014, **40**, 1–10.
- Fink, H. and Geppert, S., Implied correlation indices and volatility forecasting. *Appl. Econ. Lett.*, 2017, **24**(9), 584–588.
- Fink, H., Klimova, Y., Czado, C. and Stöber, J., Regime switching vine copula models for global equity and volatility indices. *Econometrics*, 2017, **5**(1), 855–880.
- Fleming, J., The quality of market volatility forecasts implied by S&P 100 index options. *J. Empir. Financ.*, 1998, **5**(4), 317–345.
- Fleming, J., Ostdiek, B. and Whaley, R.E., Predicting stock market volatility: A new measure. *J. Futures Markets*, 1995, **15**(3), 265–302.
- Gasser, T., Kneip, A. and Köhler, W., A flexible and fast method for automatic smoothing. *J. Am. Stat. Assoc.*, 1991, **86**(415), 643–652.
- Gradojevic, N. and Gencay, R., Predictors of triangular arbitrage opportunities: Interdependence and order book indicators. Working Paper, 2014.
- Grossmann, A., Love, I. and Orlov, A.G., The dynamics of exchange rate volatility: A panel VAR approach. *J. Int. Financ. Markets Inst. Money*, 2014, **33**, 1–27.
- Härdle, W., *Applied Nonparametric Regression*, 1990 (Cambridge University Press: Cambridge).
- Härdle, W. and Silyakova, E., Implied basket correlation dynamics. SFB 649 discussion paper, 066, 2012.
- Jung, R.C. and Maderitsch, R., Structural breaks in volatility spillovers between international financial markets: Contagion or mere interdependence? *J. Bank. Financ.*, 2014, **47**, 331–342.
- Jorion, P., Predicting volatility in the foreign exchange market. *J. Financ.*, 1995, **50**(2), 507–528.
- Jorion, P., Risk Management lessons from Long-Term Capital Management. *Eur. Financ. Manage.*, 2000, **6**(3), 277–300.

- Kim, J.S. and Seo, S.W., The information content of option-implied information for volatility forecasting with investor sentiment. *J. Bank. Financ.*, 2015, **50**, 106–120.
- Latane, H.A. and Rendleman, R.J., Standard deviations of stock price ratios implied in option prices. *J. Financ.*, 1976, **31**(2), 369–381.
- Li, M., An examination of the continuous-time dynamics of international volatility indices amid the recent market turmoil. *J. Empir. Financ.*, 2013, **22**, 128–139.
- Linders, D. and Schoutens, W., A framework for robust measurement of implied correlation. *J. Comput. Appl. Math.*, 2014, **271**, 39–52.
- Lopez, J.A. and Walter, C.A., Is implied correlation worth calculating? Evidence from foreign exchange options and historical data. *J. Deriv.*, 2000, **7**(3), 65–82.
- Ma, F., Wang, Y., Wei, Y. and Wu, C., Forecasting realized volatility in a changing world: A dynamic model averaging approach. *J. Bank. Financ.*, 2016, **64**, 136–149.
- Magris, M., Bärholm, P. and Kannainen, J., Implied volatility smile dynamics in the presence of jumps. Working Paper, 2017.
- Mixon, S., Factors explaining movements in the implied volatility surface. *J. Futures Markets*, 2002, **22**(10), 915–937.
- Mueller, P., Stathopoulos, A. and Vedolin, A., International correlation risk. *J. Financ. Econ.*, 2017, **126**(2), 270–299.
- Rebonato, R., *Volatility and Correlation: The Perfect Hedger and the Fox*, 2004 (John Wiley & Sons: Chichester, West Sussex).
- Reiswich, D. and Wystup, U., FX volatility smile construction. *Wilmott*, 2012, **0**, 58–69. doi:10.1002/wilm.10132
- Roll, R., The international crash of October 1987. *Financ. Analy. J.*, 1988, **44**(5), 19–35.
- Scott, E. and Tucker, A., Implied correlation for pricing multi-FX options. *J. Bank. Financ.*, 1989, **13**(6), 839–851.
- Siegel, A.F., International currency relationship information revealed by cross-option prices. *J. Future Markets*, 1997, **17**(4), 369–384.
- Skiadopoulos, G., Hodges, S. and Clewlow, L., The dynamics of the S&P 500 implied volatility surface. *Rev. Deriv. Res.*, 1999, **3**, 263–282.
- Skintzi, V.D. and Refenes, A.-P.N., Implied correlation index: A new measure of diversification. *J. Altern. Invest.*, 2005, **25**(2), 171–197.
- Wystup, U., How the Greeks would have hedged correlation risk of foreign exchange options. In *Foreign Exchange Risk*, edited by J. Hakala and U. Wystup, 2002 (Risk Publications: London).